ASTROMETRY, RADIAL VELOCITY, AND PHOTOMETRY: THE HD 128311 SYSTEM REMIXED WITH DATA FROM *HST*, HET, AND APT[*]

Barbara. E. McArthur[1], G. Fritz. Benedict[1], Gregory W. Henry[2], Artie Hatzes[3], William D. Cochran[1],
Tom E. Harrison[4,7], Chris Johns-Krull[5], and Ed Nelan[6]

[1] McDonald Observatory, University of Texas at Austin, Austin, TX 78712, USA; mca@astro.as.utexas.edu
[2] Center of Excellence in Information Systems, Tennessee State University, 3500 John A. Merritt Blvd., P.O. Box 9501, Nashville, TN 37209, USA
[3] Thüringer Landessternwarte, Sternwarte 5, D-07778 Tautenburg, Germany
[4] Department of Astronomy, New Mexico State, Las Cruces, NM 88003, USA
[5] Department of Physics and Astronomy, Rice University, MS-108, 6100 Main Street, Houston, TX 77005, USA
[6] Space Telescope Science Institute, 3700 San Martin Drive, Baltimore, MD 21218, USA

ABSTRACT

We have used high-cadence radial velocity measurements from the Hobby–Eberly Telescope with published velocities from the Lick 3 m Shane Telescope, combined with astrometric data from the *Hubble Space Telescope* (*HST*) Fine Guidance Sensors to refine the orbital parameters of the HD 128311 system, and determine an inclination of $55°95 \pm 14°55$ and true mass of $3.789 ^{+0.924}_{-0.432} \, M_{\rm JUP}$ for HD 128311 c. The combined radial velocity data also reveal a short period signal which could indicate a third planet in the system with an $M \sin i$ of $0.133 \pm 0.005 \, M_{\rm JUP}$ or stellar phenomena. Photometry from the T12 0.8 m automatic photometric telescope at the Fairborn Observatory and *HST* are used to determine a photometric period close to, but not within the errors of the radial velocity signal. We performed a cross-correlation bisector analysis of the radial velocity data to look for correlations with the photometric period and found none. Dynamical integrations of the proposed system show long-term stability with the new orbital parameters of over 10 million years. Our new orbital elements do not support the claims of HD 128311 b and c being in mean motion resonance.

Key words: astrometry – parallaxes – planetary systems – planets and satellites: dynamical evolution and stability – stars: individual (HD 128311, Upsilon Andromedae)

Online-only material: color figures, machine-readable tables

1. INTRODUCTION

HD 128311 is a variable K3 V (alternatively K0 V) star of BY Dra-type that is approximately 0.5 Gyr old and 16.57 pc from Earth, younger and less massive than our Sun. It is a probable member of the Ursa Major moving group (Maldonado et al. 2010). The first planet found around HD 128311, with a period of 422 days, was announced in 2003, discovered with high-precision radial velocity (RV) measurements by Butler et al. (2003), who also noted a linear trend in the data (which could also indicate and additional longer period companion). In 2005, a second planet, with a period of 928 days, was announced and a signal found at 5.6 days was attributed to starspots (Vogt et al. 2005).

The early published RV orbital parameters were unstable in dynamic integrations (Vogt et al. 2005; Meschiari et al. 2009). The suggestion was made that mean motion resonance (MMR) was a path to stability, and many studies were performed on the system in MMR (Vogt et al. 2005; Beaugé et al. 2006; Quillen 2006; Sándor & Kley 2006; Sándor et al. 2007; Michtchenko et al. 2008; Meschiari et al. 2009; Crida et al. 2008;

Lee & Thommes 2009; Voyatzis et al. 2009). Some invoked planet–planet scattering as a pathway to the resonance (Barnes & Greenberg 2006a, 2006b; Raymond et al. 2008) and some used turbulence to explain the broken apsidal corotation while the system is thought to be in MMR (Rein & Papaloizou 2009; Lecoanet et al. 2009). In addition to the most common 2:1 MMR suggestion, a retrograde MMR was explored (Gayon & Bois 2008; Gayon-Markt & Bois 2009) and, alternatively, a Trojan configuration of planets in highly inclined orbits in 1:1 MMR was proposed (Goździewski & Konacki 2006; Érdi et al. 2007) which was later suggested to be quasi-satellite trajectories instead of the Trojan configuration (Giuppone et al. 2010).

An important complement to the discovery of extrasolar planets is the discovery of disks around these multiple planet-bearing stars, which can elaborate the possibility of interactions which could produce these detectable excesses. A study searching for disks around exoplanet host stars using the criteria proposed by Mannings & Barlow (1998) identified an IR excess that may have indicated the presence of dust in a circumstellar disk around HD 128311 (Saffe & Gómez 2004). Emission was found at $70 \, \mu m$ with the *Spitzer* MIPS instrument, but no evidence for excess is seen out to $30 \, \mu m$ (Beichman et al. 2005). Using the Infrared Spectrograph (IRS) on *Spitzer*, no excess was found at $5–35 \, \mu m$ and single grain modeling projected that the disk seen at $70 \, \mu m$ must start beyond 15 AU (Beichman et al. 2006), similar to the solar system's Kuiper Belt. Trilling et al. (2008) found a fractional luminosity (f_d at $70 \, \mu m$ maximum of 2.7% and minimum of 1.3%). Bryden et al. (2009) regarded this as a relatively weak detection, with no excess at $24 \, \mu m$ detected with MIPS. *Spitzer* observations found no excess at $160 \, \mu m$ (Tanner et al. 2009). Lawler et al. (2009) found that HD 128311 was 1 of 3 stars out of 152 FGKM stars that had a $70 \, \mu m$ excess

Table 1
Mass and Radius of HD 128311

ID	Value	Unit	Reference
M_*	0.84	$M_\odot$	Vogt et al. 2005
M_*	0.828 −0.012 + 0.008	$M_\odot$	Takeda et al. 2007
R_*	0.73 ± 0.016	$R_\odot$	Valenti & Fischer 2005
R_*	0.78 ± 0.02	$R_\odot$	van Belle & von Braun 2009
R_*	0.762 ± 0.013	$R_\odot$	Ribas et al. 2003
R_*	0.76 ± 0.02	$R_\odot$	Takeda et al. 2007

without a corresponding excess at 33 μm. The detection of the cool dust at 70 μm in HD 128311, indicates that there are most likely still collisions in this system, coming from the interaction of large planetesimal, small undetected planetary perturbers, or from effects of interactions of the known planets.

HD 128311 is one of the handful of systems (currently six; Moro-Martín et al. 2010) known to contain planets and debris disks, which further enhances its role in the study of formation and evolution of extrasolar planetary systems. Like ϵ Eridani and HD 69830, HD 128311 also has an extensive debris belt (Trilling et al. 2008) at a radius of >5.1 AU. Moro-Martín et al. (2010) used *Spitzer* IRS spectra to predict that the location of planetesimals in the system was between 52 and 100 AU, while their dynamical modeling indicated two regions of stability for planetesimal lifetimes: interior to 0.3 AU and exterior to 4 AU, which is preferred because there is no excess emission at $\lambda < 33\,\mu$m.

Because extrasolar planetary systems are expected to produce low-frequency radio emissions, as we detect in our own planetary system, a search was made for these emissions from the planets around HD 128311 (George & Stevens 2007). No detection was found, but an upper limit of 15.5 mJy for radio emissions was placed on the system.

We have used the *Hubble Space Telescope* (*HST*) Fine Guidance Sensor (FGS) 1r to obtain millisecond of arc per observation precision astrometry which we combine with new Hobby–Eberly Telescope (HET) RVs and archival Lick velocity sets. In this paper, we use the combined astrometric and spectroscopic measurements to calculate the actual mass of planet c, show evidence of a third shorter period planet or star phenomenon, and examine the resonance and stability of the system. We use T12 automatic photometric telescope (APT) and *HST* photometry to investigate the stellar activity in this system.

2. STELLAR PROPERTIES

HD 128311 (=V* HN Boo = HIP71395 = GJ3860+RX J1436.0+0944) is a $V = 7.446$, K3V star with a mass of 0.828 $M_\odot$ and radius of 0.76 $M_\odot$ (see Table 1). Table 2 summarizes the observed properties of HD 128311, a star with roughly solar metallicity. Observations of Ca II H and K lines indicate high chromospheric activity for this star (Butler et al. 2003; Vogt et al. 2005). Butler's initial estimates of photospheric velocity variability were between 30 and 100 m s^{-1} (Butler et al. 2003). Later estimates suggested the variability (sometimes referred to as jitter) was 8.9 m s^{-1} (Vogt et al. 2005). The Ca II H and K lines also showed strong emission reversals in the High Resolution Echelle Spectrometer spectra, which implies a young age of 0.5–1.0 Gyr (Vogt et al. 2005). All age estimates can be seen in Table 3. Though we have chosen specific measurements to use in our calculations we list alternative measurements for ease of comparison, and disclosure of the star properties.

Table 2
Stellar Properties of HD 128311

ID	Value	Unit	Reference
Spectral type	K3 V	. . .	Gray et al. 2003
Spectral type	K0 V	. . .	Vogt et al. 2005
$v \sin i$	3.65	km s^{-1}	Fischer & Valenti 2005
A_V	0.59 ± 0.013	mag	van Belle & von Braun 2009
B	8.55	mag	Bailer-Jones 2011
V	7.51 ± 0.05	mag	Bailer-Jones 2011
R	6.88	mag	Zacharias et al. 2004
I	6.711	mag	Droege et al. 2006
J	5.772 ± 0.018	mag	Bailer-Jones 2011
H	5.303 ± 0.031	mag	Bailer-Jones 2011
K	5.142 ± 0.017	mag	Bailer-Jones 2011
$T_{\rm eff}$	4815 ± 53	K	Ramírez & Meléndez 2005
$T_{\rm eff}$	4965	K	Valenti & Fischer 2005
$T_{\rm eff}$	4763	K	Saffe et al. 2008[a]
$\log g$	4.83 ± 0.1	cm s^{-2}	Valenti & Fischer 2005
$\log g$	4.61 −0.02 + 0.01	cm s^{-2}	Takeda et al. 2007
[Fe/H]	0.2	dex	Valenti & Fischer 2005
[Fe/H]	0.1	dex	Ramírez & Meléndez 2005
[Fe/H]	0.023 ± 0.081	dex	Gonzalez & Laws 2007
X-ray flux	10.2 ± 1.35	10^{-13} erg cm^{-2} s^{-1}	Kashyap et al. 2008

Note. [a] Castelli et al. (1997) calibration.

Table 3
Age Estimates of HD 128311

ID	Value	Unit	Reference
Age	<0.39	Gyr	Saffe et al. 2005[a]
Age	<0.41	Gyr	Saffe et al. 2005[b]
Age	<6.4	Gyr	Valenti & Fischer 2005
Age	<0.960 ± 0.04	Gyr	Barnes 2007[c]
Age	0.351	Gyr	Barnes 2007[d]
Lower age limit	<0.7	Gyr	Valenti & Fischer 2005
Upper age limit	<12.7	Gyr	Valenti & Fischer 2005
Upper age limit	<0.96	Gyr	Takeda et al. 2007

Notes.
[a] Chromospheric age using the calibration of Donahue (1993).
[b] Chromospheric age using the calibration of Rocha-Pinto & Maciel (1998).
[c] Isochrone age.
[d] Gyrochronology used for age.

3. OBSERVATIONS, DATA REDUCTION, AND MODELING

3.1. HET and Lick Radial Velocity Observations

The High Resolution Spectrograph (HRS; Tull 1998) at the HET at McDonald Observatory was used to make the spectroscopic observations using the iodine absorption cell method (Butler et al. 1996). Our reduction of HET HRS data is given in Bean et al. (2007), which uses the REDUCE package (Piskunov & Valenti 2002). Our observations include a total of 355 high-resolution spectra which were obtained between 2005 April and 2011 January. Because typically two or more observations were made in less than 1 hr per night, we observed at 161 epochs with the HET HRS.

Our HET RV data set was combined with overlapping velocities from Lick taken from Meschiari et al. (2009) to produce a total data set that spans 13 yr. The total RV data set contained 455 observations of HD 128311. Table 4 contains reduced HET velocities for the observed epochs. We removed a few HET RV observations from our data set based upon the analysis discussed in Section 4.4.
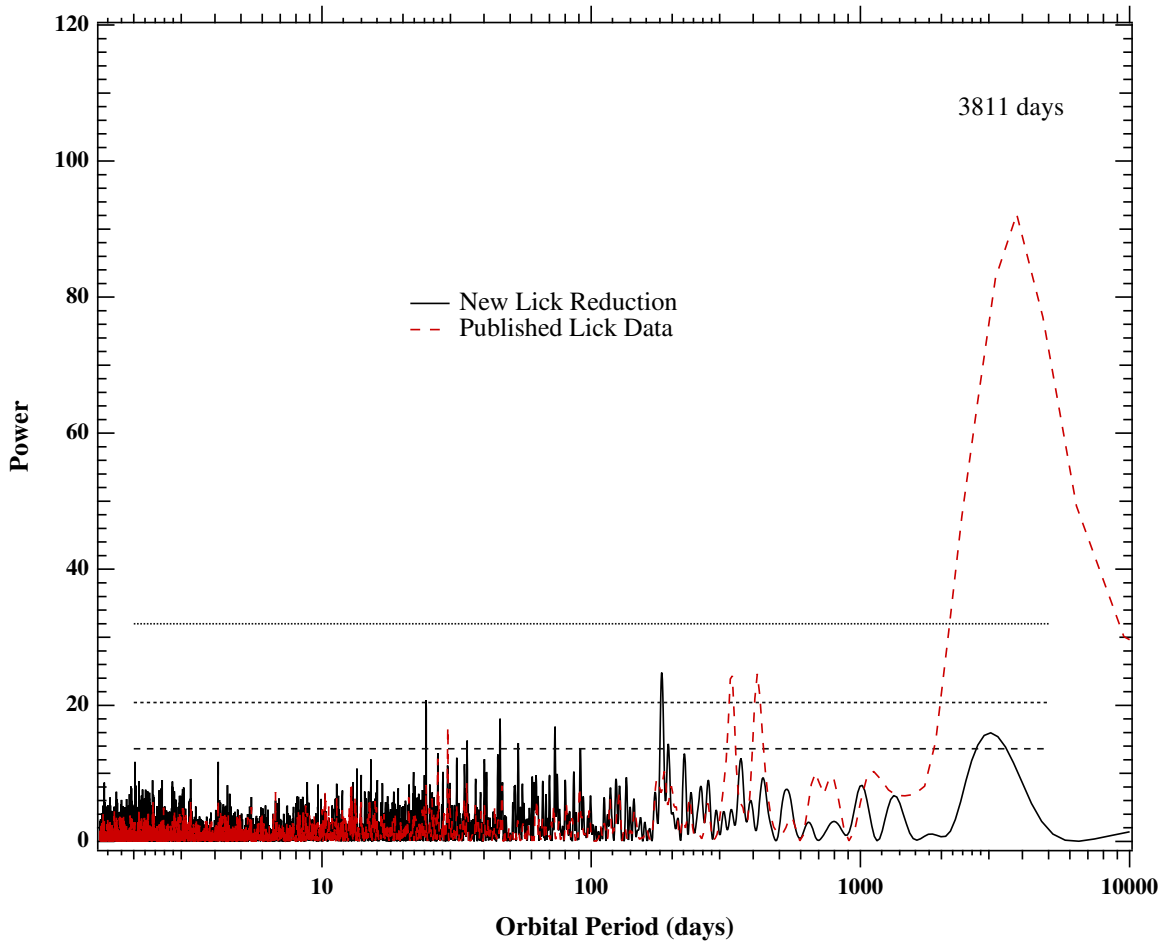
Figure 1. Periodogram of the radial velocities of υ Andromedae from two reductions of Lick data: the published (Wright et al. 2009) and the new lick reduction (D. Fisher & M. Giguere 2009, private communication). Shows the two periodogram of the residuals to a Keplerian model that contains the planet b (period 4.617 days), planet c (241 days), and planet d (1282 days). The significance of the signal at 3811 days (identified as υ Andromedae by Curiel et al. 2011) is considerably diminished in the new Lick reduction. The dotted lines show the significance levels of the power in each plot, from the top: 1.0e10, 1.0e5, and 1.0e2.

(A color version of this figure is available in the online journal.)

Table 4
HET Relative Radial Velocities for HD 128311

JD− 2450000	RV (m s^{-1})	± Error[a]
3462.965290	97.99	6.99
3479.731833	82.71	6.97
3479.899542	84.95	6.97
3480.919038	93.96	7.11
3482.891047	80.4	7.21

Notes.
[a] Errors as modeled; no additional noise error to be added.

(This table is available in its entirety in a machine-readable form in the online journal. A portion is shown here for guidance regarding its form and content.)

3.1.1. Lick Radial Velocity Observation Adjustments

For our study of υ Andromedae (McArthur et al. 2010), Fischer and Giguere forwarded us re-reduced velocities for υ Andromedae from Lick Observatory. They had improved the pipeline and included additional γ offsets that were related to the use of different detectors on the instrument (D. Fischer & M. Giguere 2009, private communication). The earlier Lick data for υ Andromedae (Wright et al. 2009) contained a signal at 3811 days which was not present in their re-reduced γ adjusted data set as shown in Figure 1. This instrumental signal in the

data created by neglected γ offsets was identified as a fourth planet with period of 3848 days and possibly in resonance with υ Andromedae c in Curiel et al. (2011). Since the time span of the observations of the system was less than 1.5 cycles of this long-period signal, the instrumental effect on the data set was not revealed. In a Bayesian analysis of the separate reductions of the Lick velocities for υ Andromedae (Fischer et al. 2003; Wright et al. 2009), Tuomi et al. (2011) concluded that there were large inconsistencies (700 days) in the period determination of the proposed υ Andromedae e, based upon which Lick reduction was used in the analysis, which caused them to question the source of the fourth signal (bias or Keplerian signal).

While re-reduction of the Lick library is forthcoming (D. Fischer 2010, private communication) it has not been published at the time of this investigation so we included four independent γ offsets in our fitting of the HD 128311 velocities that related to the timing of the detector changes. These γ offsets and the time periods and number of observations in the fit (of the γ offset) in the Lick velocities are shown in Table 5.

Additionally, we also considered two independent reductions of the Lick velocities—the set in Butler et al. (2006) and the set in Meschiari et al. (2009). When we compared the velocities, using only the data after the last Lick detector change (post-Julian Date 2452515), we found a small yearly signal difference (as a function of day of the year) between the two sets shown
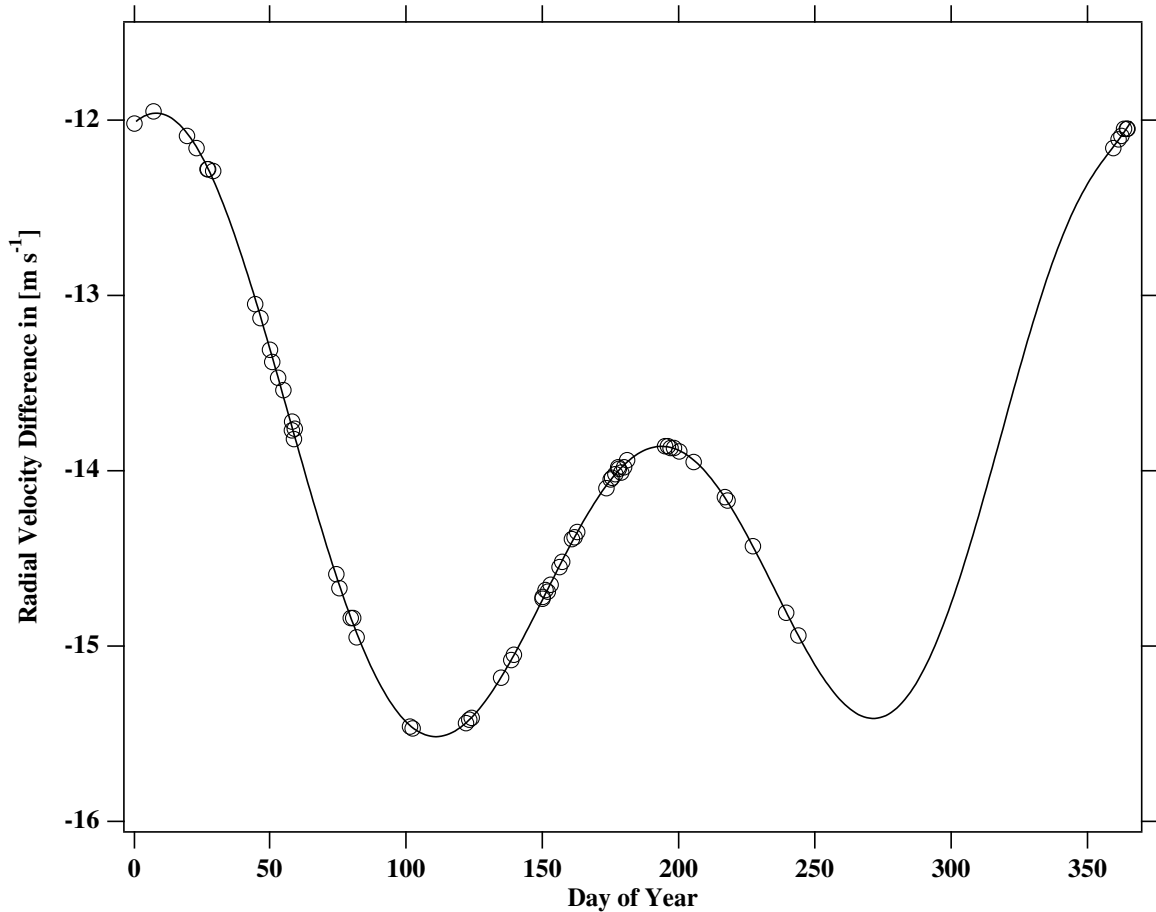
Figure 2. RV difference in the two reductions (Butler et al. 2006; Meschiari et al. 2009) of Lick HD 128311 data phased to 1 yr are shown by the open circles. The solid line is a polynomial that was fit to the difference and applied to the newer data set.

Table 5
γ Offsets for Lick Radial Velocities of HD 128311

Julian Date (Start)	Julian Date (End)	Number of Velocities	γ	$\pm$ Error
2450983	2451371	4	0.85	2.44
2451409	2452163	14	4.80	5.34
2452333	2452489	9	1.16	3.60
2452515	2454602[a]	64	3.44	1.19

Note. [a] Observation date of last Lick velocity included in this analysis, not necessarily the end date for this γ value.

in Figure 2. We fit this difference with a polynomial, and adjusted the more recent data set (Meschiari et al. 2009) with the polynomial. We found a slightly reduced χ^2 with the more recent (Meschiari et al. 2009) data set adjusted with the polynomial, and used this set of data in our solution.

3.2. HST Astrometry Observations

The astrometric observations were made with the *HST* FGS 1r, a two-axis interferometer, in position (POS) "fringe-tracking" mode.[8] The FGS instrument is described in Nelan (2007). Benedict et al. (2007) describes the reduction and calibration of the data. All FGS data was calibrated with a new improved Optical Field Angle Distortion (OFAD) derived by

McArthur, which is not yet unpublished, but available with the reduction pipeline. The astrometric data used in this research are available from the *HST* Program Schedule and Information Web site,[9] in proposal numbers 11210 and 11788. The two part pipeline used to reduce the raw data to the values used in this modeling is available with the latest calibration parameters from the Space Telescope Science Institute in IRAF STSDAS and in a stand-alone version available from one of the coauthors, the *HST* FGS Instrument Scientist at STSCI Ed Nelan.

FGS astrometric data are obtained by download from the *HST* online archival retrieval system and then processed through the FGS pipeline system. The initial calibration pipeline extracts the astrometry measurements (typically 1–2 minutes of fringe position information acquired at a 40 Hz rate, which yields several thousand discrete measurements) and calculates the median (after outlier removal) and performs error estimation. The second calibration stage applies the time-variant OFAD, corrects the velocity aberration, processes the time tags, and uses the JPL Earth orbit predictor (Standish 1990) to calculate the parallax factors. The form of the OFAD calibration is discussed in several calibration papers (McArthur et al. 1997, 2002, 2006). Ongoing stability tests (LTSTABs) are used to maintain this calibration. Instrumental systematics in FGS 1r (such as intra-orbit drift and color and filter effects) and their corrections are discussed in later sections. After 20 yr of calibration we have not found additional systematics in our data at a level that is higher than our detection limit. With the exception of

---

[8] A detailed Instrument Handbook can be found on the Space Telescope Science Institute Web site:
http://www.stsci.edu/hst/fgs/documents/instrumenthandbook/.

[9] http://www.stsci.edu/hst/scheduling/program_information
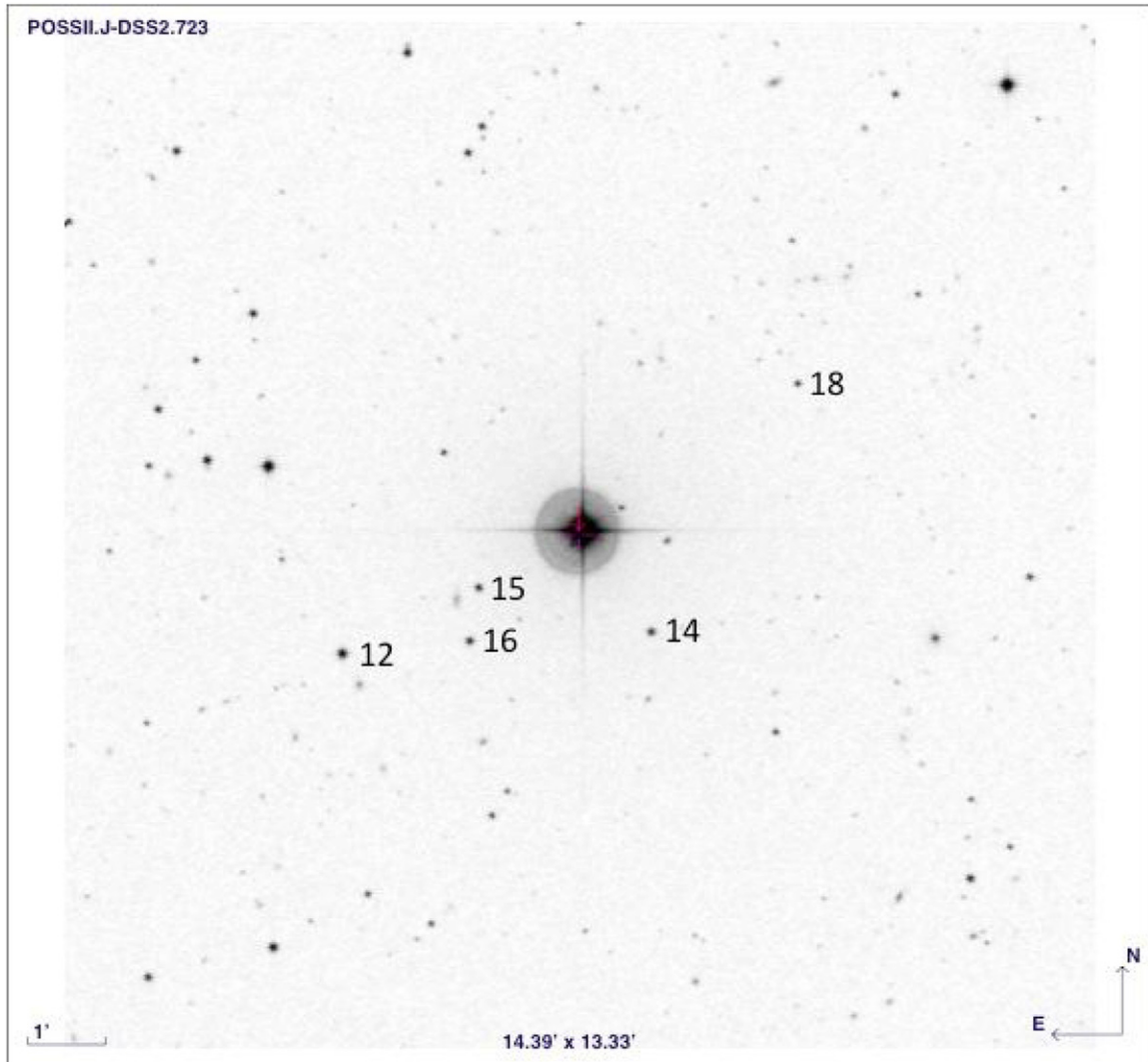
Figure 3. HD 128311 field with astrometric reference stars marked. The stars are listed in Table 11. The DSS image was secured using *Aladin*.
(A color version of this figure is available in the online journal.)

the Pleiades, regression analysis between *Hipparcos* and *HST* parallax measurements has shown not only good agreement between the determined parallaxes but an overestimation of error in *HST* astrometric measurements (Benedict et al. 2007; McArthur et al. 2010).

Twenty-nine orbits of *HST* astrometric observations were made between 2007 December and 2009 August. Because of observing constraints, there was a 225 day gap in observations between 2008 May and 2009 January. Every orbit contains several observations of HD 128311 and surrounding reference stars. The distribution of the reference stars in the HD 128311 field is shown in the Digital Sky Survey (DSS) image in Figure 3. The FGS measures the position of each star sequentially. Each epoch contains multiple visits, alternating between the target (HD 128311) and the five reference stars, providing $x(t)$ and $y(t)$ positions in the *HST* reference frame in seconds of arc. Observations during an orbit were corrected for slow FGS intra-orbit positional drift by using an adaptable polynomial fitting routine amplified to model the high intra-orbit drift seen in some of these observations. Because HD 128311 is a bright star ($V = 7.39$) a neutral density filter (F5ND) was used. For the reference stars the *F583W* filter was used. The dates of observation, the number of measurements of HD 128311 for

each date, the *HST* orientation angles and the number of plate parameters are listed on Table 6. The *HST* astrometric data for HD 128311 and its reference stars is available only online (Table 7). For the most current calibration the data should be retrieved from the *HST* online archival retrieval system and processed through the two stage pipeline system.

3.3. Spectrophotometric Parallaxes for the Reference Stars

An *HST* target parallax is relative with respect to its reference frame. To go from relative to absolute parallax for HD 128311, we can either apply a statistically derived correction from relative to absolute parallax (van Altena et al. 1995; compare to Yale Parallax Catalog, YPC95), or use a Bayesian approach in which we use the derived spectroscopic parallaxes of the reference frame stars as input to the model. We estimate the absolute parallaxes of the reference frame stars from the colors, spectral type, and luminosity classes of the stars. We require the absolute magnitude, M_V, and V-band absorption, A_V for the equation

$$\pi_{abs} = 10^{-(V-M_V+5-A_V)/5}. \tag{1}$$

Our model then produces an absolute, not relative parallax.

Table 6
HST Astrometric Observations of HD 128311 and the Reference Frame

Orbit	Year	Day	Julian Date	N_{obs}	*HST* Roll
1	2007	360	2454461.32336805	3	238.7345
2	2007	364	2454464.51170138	4	239.3361
3	2008	6	2454471.50753472	4	239.7188
4	2008	25	2454491.22082175	4	238.9152
5	2008	32	2454498.41331018	4	239.9798
6	2008	38	2454503.80822916	4	256.6916
7	2008	43	2454509.26917824	4	258.6858
8	2008	49	2454514.59637731	4	261.1828
9	2008	55	2454520.52322916	4	264.1754
10	2008	62	2454528.38375000	4	265.9971
11	2008	68	2454534.31335648	4	265.9971
12	2008	76	2454542.23754629	4	276.9977
13	2008	83	2454548.69702546	4	276.9977
14	2008	87	2454553.36010416	4	276.9977
15	2008	103	2454569.14370370	4	330.2641
16	2008	121	2454587.06107639	4	335.0302
17	2008	131	2454597.11729166	4	20.03228
18	2008	140	2454605.84104166	4	24.03138
			Servicing mission		
19	2009	1	2454832.61401620	4	235.9564
20	2009	38	2454870.30037037	4	256.7992
21	2009	46	2454877.82504629	4	238.9172
22	2009	65	2454896.60428240	4	268.9989
23	2009	83	2454915.25145833	4	268.9952
24	2009	96	2454928.03842592	4	283.9783
25	2009	117	2454949.01655092	4	340.0253
26	2009	163	2454994.56111111	4	31.02961
27	2009	190	2455022.05805555	4	79.0068
28	2009	204	2455036.44101851	4	81.00542
29	2009	222	2455053.81746527	4	81.00542

3.3.1. Reference Star Photometry

Our bandpasses for reference star photometry include: BV (CCD photometry from a 1 m telescope at New Mexico State University),[10] *V* (from FGS 1r), and *JHK* from Two Micron All Sky Survey.[11] The *JHK* values have been transformed to

---

[10] The Apache Point Observatory 3.5 m telescope is owned and operated by the Astrophysical Research Consortium.
[11] The Two Micron All Sky Survey is a joint project of the University of Massachusetts and the Infrared Processing and Analysis Center/California Institute of Technology.

---

the Bessell & Brett (1988) system using the transformations provided in Carpenter (2001). Table 8 lists *VJHK* photometry for the target and reference stars indicated in Figure 3. Figure 4 contains a $(J - K)$ versus $(V - K)$ color–color diagram with reference stars and HD 128311 labeled.

3.3.2. Spectroscopy, Luminosity Class, and Reduced Proper Motion

The derived absolute magnitudes are critically dependent on the assumed stellar luminosities, a parameter impossible to obtain for all but the latest type stars using only Figure 4. The spectra from which we estimated spectral type and luminosity class come from the Cerro Tololo Inter-American Observatory 4 m with RCSPEC. The KPGL1-1 grating was used in first order, which has 632 l mm^{-1}, blaze wavelength 4200 Å and a 150 μm slit ($=1''$). The dispersion was 1.0 Å pixel^{-1} with wavelength coverage from 3500 to 5850 Å. Classifications used a combination of a large library of MK templates for matching and line ratios. The faintest target (REF-6) had about 4000 peak counts in the continuum above sky per pixel, or signal-to-noise ratio (S/N) $\sim$ 60. While the S/N was very high and the matching library substantial, we found that the resulting instrumental resolution limited our spectral classification to ± 2 subclasses. The field had very low extinction $A_v \leqslant 0.1$ for all stars.

To confirm the luminosity classes, we obtain PPMXL proper motions (Roeser et al. 2010) for a one-degree-square field centered on HD 128311 shown in Figure 5, and then iteratively employ the technique of reduced proper motion (Yong & Lambert 2003; Gould & Morgan 2003) to discriminate between giants and dwarfs.

3.3.3. Estimated Reference Frame Absolute Parallaxes

We derive spectrophotometric parallaxes using our estimated spectral types and luminosity class and M_V values from Cox (2000). Our adopted input errors for distance moduli, $(m - M)_0$, are 0.4 mag for all reference stars. Contributions to the error are a small but undetermined A_V and in M_V errors due to uncertainties in color to spectral type mapping. All reference star absolute parallax estimates, spectral types and luminosities are listed in Table 9. Individually, no reference star absolute parallax is better determined than $(\sigma_\pi/\pi) = 18\%$. The average input absolute parallax for the reference frame is $\langle \pi_{abs} \rangle = 0.7$ ms of arc (mas), a quantity known to $\sim 40\%$ (standard deviation
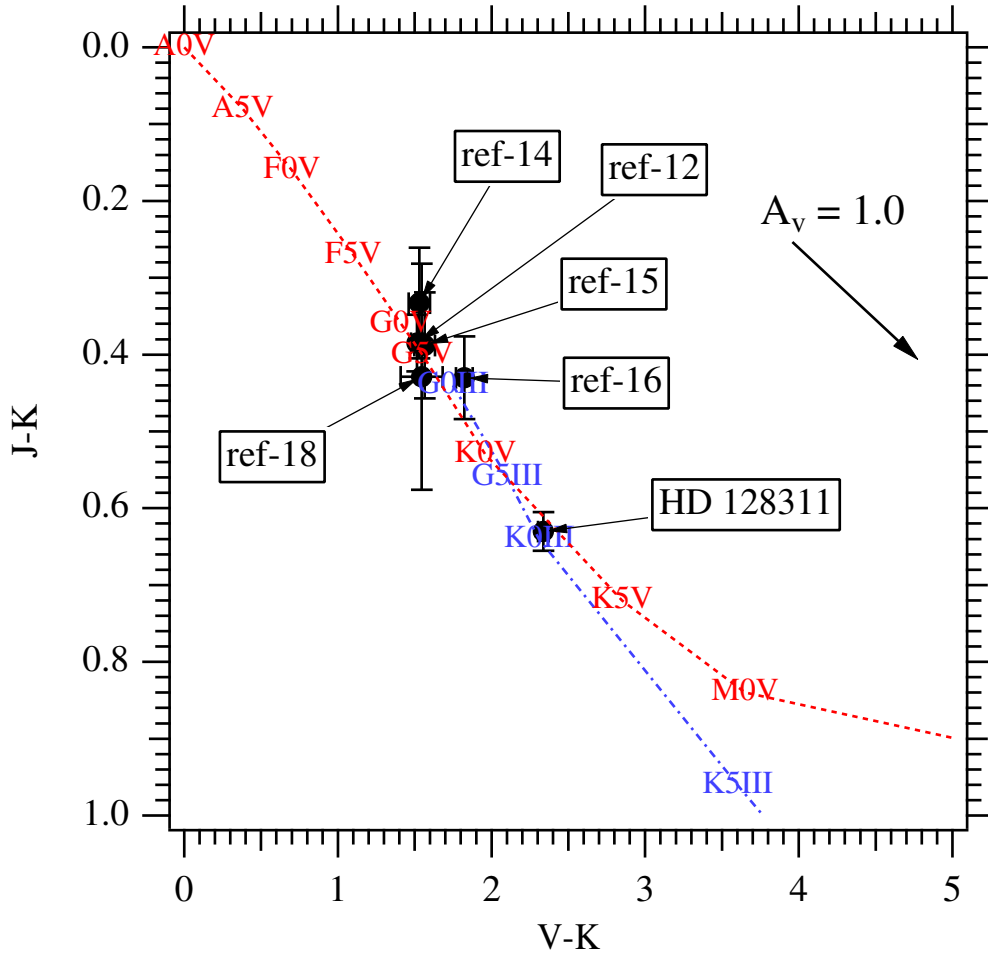
Table 7
HST Astrometric Data for HD 128311 and Reference Stars

Set	ObsID	Star	rollV3	Filter	Xmad	Ymad	Xvaofadapj2d	Yvaofadapj2d
1	F9YM1902M	16	238.7345	F583W	0.00295	0.0024	-112.8103	755.9297

(This table is available in its entirety in a machine-readable form in the online journal. A portion is shown here for guidance regarding its form and content.)

Table 8
V and Near-IR Photometry of HD 128311 and Reference Stars

ID	*V*	*K*	$(J - H)$	$(J - K)$	$(V - K)$
2	7.48 ± 0.03	5.142 ± 0.017	0.469 ± 0.036	0.630 ± 0.025	2.338 ± 0.0345
12	14.15 ± 0.03	12.635 ± 0.026	0.280 ± 0.040	0.385 ± 0.037	1.515 ± 0.040
14	15.45 ± 0.03	13.92 ± 0.063	0.297 ± 0.055	0.333 ± 0.072	1.53 ± 0.070
15	15.62 ± 0.03	14.056 ± 0.06	0.375 ± 0.051	0.388 ± 0.069	1.564 ± 0.067
16	15.29 ± 0.03	13.466 ± 0.045	0.368 ± 0.042	0.430 ± 0.054	1.824 ± 0.054
18	16.5 ± 0.03	14.955 ± 0.133	0.373 ± 0.091	0.429 ± 0.147	1.545 ± 0.136

Figure 4. $(J - K)$ vs. $(V - K)$ color–color diagram for stars in the HD 128311 field identified in Table 8. The dashed line is the locus of dwarf (luminosity class V) stars of various spectral types; the dot–dashed line is for giants (luminosity class III). The reddening vector indicates $A_V = 1.0$ for the plotted color systems. Along this line of sight maximum extinction is $A_V \sim 0.3$ (Schlegel et al. 1998).

(A color version of this figure is available in the online journal.)

Table 9
Astrometric HD 128311 Reference Star Adopted
Spectrophotometric Parallaxes

ID	Sp. T.[a]	V	$B - V$	M_v	A_v	π_{abs} (mas)
12	G0V	14.15	0.59 ± 0.03	4.20	0.07	1.066 ± 0.267
14	G1V	15.45	0.61 ± 0.07	4.24	0.06	0.594 ± 0.148
15	G1V	15.62	0.54 ± 0.08	4.24	0.06	0.553 ± 0.138
16	G4V	15.29	0.69 ± 0.07	4.82	0.10	0.882 ± 0.220
18	G1V	16.50	0.61 ± 0.11	4.24	0.10	0.371 ± 0.093

Note. [a] Spectral types and luminosity class estimated from colors and reduced proper motion diagram.

of the mean of five reference stars). We compare this to the correction to absolute parallax discussed and presented in YPC95 (Section 3.2, Figure 3). Entering YPC95, Figure 3, with the Galactic latitude of HD 128311, $b = +59°.85$, and average magnitude for the reference frame, $\langle V_{ref} \rangle = 15.4$, we obtain a correction to absolute parallax of 1.3 mas, with is higher than our average input parallax, but derived from a compressed portion of the YPC graph. Nonetheless, rather than apply a model-dependent correction to absolute parallax, we introduce our spectrophotometrically estimated reference star parallaxes into our reduction model as observations with error.

Table 10
Astrometric HD 128311 Reference Star Proper Motions

	Input (PPMXL)		Final (*HST*)	
ID	μ_α[a]	μ_δ[a]	μ_α	μ_δ
12	-6.2 ± 3.6	-6.0 ± 3.6	-8.17 ± 0.38	-8.59 ± 0.34
14	-4.5 ± 3.6	-5.2 ± 3.6	-5.02 ± 0.37	-6.12 ± 0.33
15	-7.5 ± 3.6	4.4 ± 3.6	-7.79 ± 0.39	8.28 ± 0.34
16	54.3 ± 3.6	-5.1 ± 3.6	-52.08 ± 0.33	-7.72 ± 0.27
18	3.0 ± 3.8	3.6 ± 3.8	2.92 ± 0.85	1.53 ± 0.71

Note. [a] μ_α and μ_δ are relative motions in milliseconds of arc yr^{-1}.

3.3.4. Estimated Reference Frame Proper Motions

Typically, we use proper motion values from UCAC3 (Zacharias et al. 2009) or the PPMXL catalog (Roeser et al. 2010) as observations with error in the model. For this field we find better observational fits with the PPMXL catalog data, with a vector offset in the UCAC3 catalog. The PPMXL proper motions, the reference frame derived values and our final model values are found in Table 10.

3.4. Astrometric Model

The HD 128311 reference frame contained five reference stars plus HD 128311. *HST* rolls with the observations, so
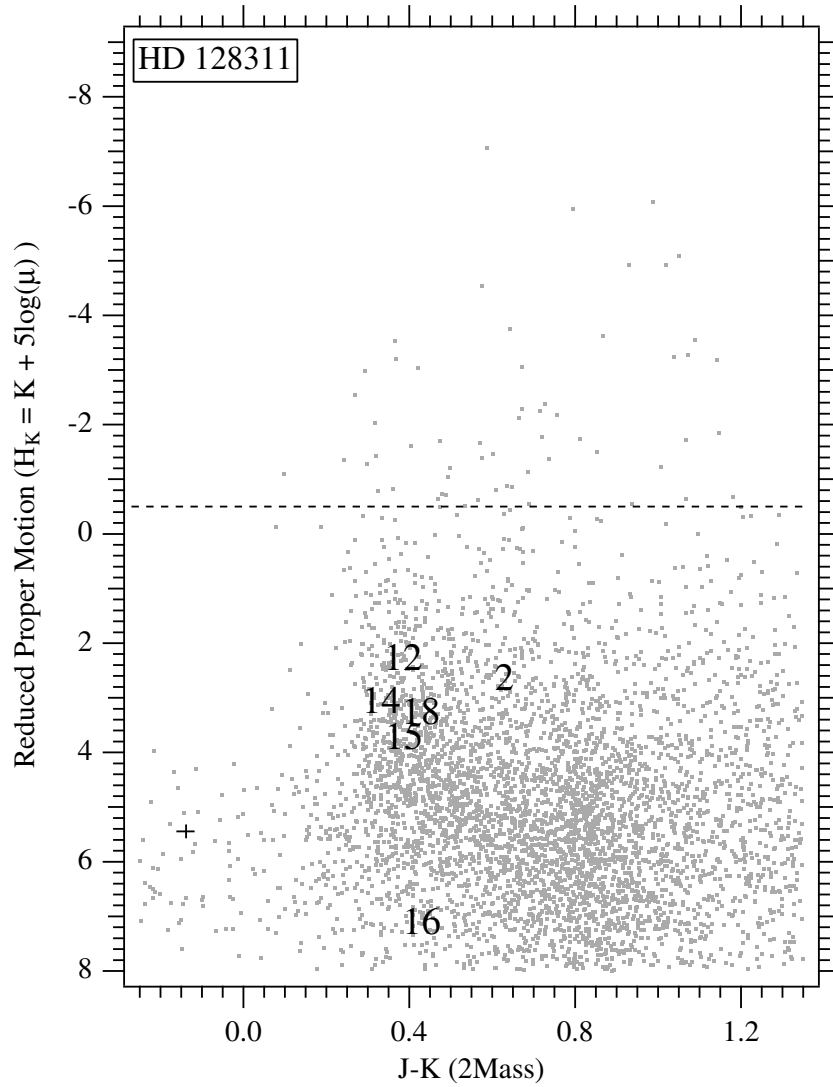
Figure 5. Reduced proper motion diagram for 5800 stars in a $1°$ field centered on HD 128311. Star identifications are in Table 8. For a given spectral type, giants and sub-giants have more negative H_K values and are redder than dwarfs in $(J - K)$. H_K values are derived from "final" proper motions in Table 10. The small cross at the lower left represents a typical $(J - K)$ error of 0.04 mag and H_K error of 0.17 mag. The horizontal dashed line is a giant-dwarf demarcation derived from a statistical analysis of the *Tycho* input catalog (D. R. Ciardi 2004, private communication).

the positions (x', y') of the target and reference stars change with each observation set. We use an overlapping plate model that includes parameters for scale, rotation, and offset. Each plate expresses its relation to the constraint or master plate, usually one of the central observations, with these parameters. The astrometric model also accounts for the movements of each star, which are time-dependent, given by the absolute parallax π_{abs} and the proper motion components, μ_α and μ_δ. We include instrumentally caused position shift parameters for the cross-filter and lateral color. The standard coordinate catalog positions ξ and η are the result of modeling these equations of condition:

$$x' = x + lc_x(B - V) - \Delta\text{XF}x, \qquad (2)$$

$$y' = y + lc_x(B - V) - \Delta\text{XF}y, \qquad (3)$$

$$\xi = Ax' + By' + C - \mu_\alpha\Delta t - P_\alpha\pi - \text{ORBIT}_x, \qquad (4)$$

$$\eta = -Bx' + Ay' + F - \mu_\delta\Delta t - P_\delta\pi - \text{ORBIT}_y, \qquad (5)$$

where x and y are the measured coordinates from *HST*; lc_x and lc_y are the lateral color corrections, and $B - V$ are the $B - V$ colors

of each star; $\Delta\text{XF}x$ and $\Delta\text{XF}y$ are the cross-filter corrections in x and y, applied only to the observations of HD 128311. A and B are scale and rotation plate constants, and C and F are offsets, μ_α and μ_δ are proper motions, Δt is the epoch difference from the mean epoch, P_α and P_δ are parallax factors, and π is the parallax. We obtain the parallax factors from a JPL Earth orbit predictor Standish (1990), upgraded to version DE405. ORBIT is a function using Thiele–Innes constants (Heintz 1978) of the traditional astrometric and RV orbital elements. We used a model written in the GaussFit language (Jefferys et al. 1988) employing robust estimation to derive a simultaneous solution. Table 11 shows the resulting astrometric catalog from the combined orbital modeling.

Additionally, equations of condition relate an initial and final parameter value. For the reference stars there are equations in the model for proper motion and spectrophotometric parallax. For the target star (HD 128311) we add equations for cross-filter. Both target and reference stars have equations for lateral color parameters. The roll of the constraint plate also has a condition equation. Through these additional equations of condition the χ^2 minimization process is allowed to adjust

Table 11
Astrometric Catalog of HD 128311 and Reference Stars

Star	Mag V	R.A.[a] (deg)	Decl.[a] (deg)	ξ[b] (arcsec)	σ_ξ (arcsec)	η (arcsec)	σ_η (arcsec)
HD 128311	7.39	219.00281	9.74596	−1.11484	0.00011	731.65337	0.00011
12	14.15	219.05321	9.72182	151.39824	0.00019	859.97773	0.00020
14	15.44	218.98751	9.72575	43.39602	0.00017	652.54731	0.00017
15	15.58	219.02412	9.73521	64.64370	0.00019	785.18893	0.00021
16	15.3	219.02604	9.72411	104.17150	0.00016	774.82462	0.00015
18	16.54	218.95594	9.77737	−171.82461	0.00050	625.47534	0.00051

Notes.
[a] Predicted coordinates for equinox J2000.0.
[b] Relative coordinates in the reference frame of the constrained plate (set 18, with roll = 24°03138).

parameter values by amounts constrained by the input errors. In this quasi-Bayesian approach prior knowledge is input as an observation with associated error, not as a hardwired quantity known to infinite precision. For HD 128311 no priors were used for parallax or proper motion or the orbital motion.

3.4.1. Astrometric Reference Frame Residual Assessment

The reference frame stars are modeled without HD 128311 many times to assess plate models, prior knowledge of spectrophotometric parallaxes, catalog proper motions, and stability as a reference star. We plotted reference frame x and y residuals against a number of spacecraft, instrumental, and astronomical parameters. These included x and y position within our total field of view, radial distance from the field-of-view center, reference star V magnitude and $B − V$ color, and epoch of observation. We saw no trends indicating systematic instrumental effects that were larger than 1 mas. There is a predicted small upward trend in residuals with the faintest star.

3.4.2. Astrometric Catalog Residual Assessment

HST FGS 1r has raw distortions of more than $1''$, but the OFAD (McArthur et al. 2002) calibration reduces these distortions to below 2 mas over much of the FGS 1r field. Histograms of the astrometric residuals (Figure 6) show the goodness of the fit. The astrometric catalog shown in Table 11 has ξ and η standard coordinates determined with average position errors $\langle\sigma_\xi\rangle = 0.13$ and $\langle\sigma_\eta\rangle = 0.11$ mas. The median average deviations of these positions are $\xi_{MAD} = 0.066$ and $\eta_{MAD} = 0.056$ mas.

3.5. Radial Velocity Model

We model the radial ($\hat{z}$) motion of the stellar orbital movement around the barycenter of the HD 128311 system. The equation used is a projection of a Keplerian orbital velocity to observer's line of sight plus a constant velocity offset:

$$\cos vw = \frac{\cos(E) - e}{1 - (e \times \cos(E))} \times \cos(\omega)$$
$$- \frac{\sqrt{1 - e^2} \times \sin E}{1 - (e \times \cos(E))} \times \sin(\omega), \qquad (6)$$

$$Z = \gamma + K1 \times (ecc \times \cos(\omega) + \cos vw), \qquad (7)$$

where e is eccentricity, ω is the longitude of per astron, $K1$ is the semi-amplitude of the RV signal, E is the eccentric anomaly from Kepler's equation, and γ is the constant velocity offset. We model three planetary orbits and five γ's, one for the HET and four for the Lick data.

3.6. Combined Orbital Model

For the combined orbital model, we use a linear combination of three unperturbed Keplerian orbits, which is an acceptable first-order approximation of the orbital elements, and we model one of these astrometrically (the other two orbital perturbations are below the detection limit of the *HST* FGS. Additionally, we constrain a relationship between the astrometry and the RV through this equation (Pourbaix & Jorissen 2000):

$$\frac{\alpha \sin i}{\pi_{abs}} = \frac{P K (1 - e^2)^{1/2}}{2\pi \times 4.7405}, \qquad (8)$$

where quantities only derivable from the astrometry (parallax, π_{abs}, primary perturbation orbit size, α, and inclination, i) are on the left, and quantities derivable from both (the period, P, and eccentricity, e), or RVs only (the RV amplitude of the primary, K), are on the right. The parallax, proper motion, and orbital elements were all the result of using the combined orbital model in which there was simultaneous modeling of the *HST* astrometry and RVs from Lick and the HET. Our long-term stability tests performs a full computation of perturbed orbits, which is shown in Section 4.5.

4. RESULTS

4.1. HST Parallax and Proper Motions of HD 128311

We find a parallax of 60.532 ± 0.149 mas for HD 128311. This parallax lies between the parallaxes determined with the two solutions of the *Hipparcos* data, with an error five times lower (Perryman et al. 1997; van Leeuwen 2007). We find $\mu_x = 204.963 \pm 0.162$ and $\mu_y = −249.760 \pm 0.143$. These proper motions agree with *Hipparcos* and PPMXL values, but the *HST* motions have smaller uncertainties. *HST* proper motions are relative to the reference frame. No a priori values for proper motion and parallax were used as input for HD 128311, only for the reference frame. These results are shown in Table 12, including independently determined values for comparison.

4.2. Orbital Solution

4.2.1. Radial Velocity Periodograms and Bootstrap Randomization

Until this work, the most recent published orbital solution of HD 128311 was presented in Meschiari et al. (2009). It included newer Lick velocities and HET velocities taken from Wittenmyer et al. (2009). The best-fit Newtonian orbital parameters from this fit produces a system that loses stability in the first 1000 yr. We model these same Lick values but adjusted for additional γ offsets (see Section 3.1.1) combined with our HET
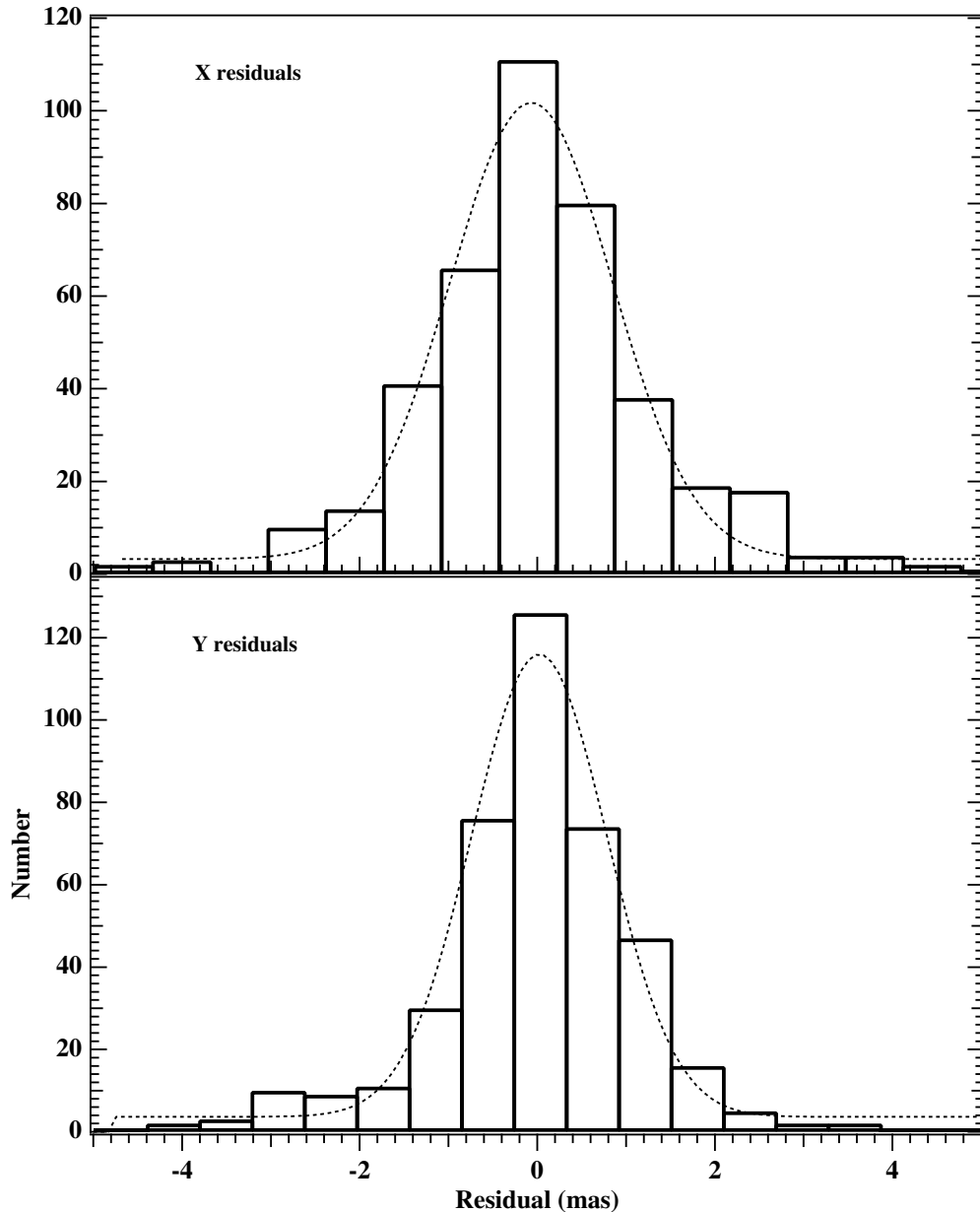
Figure 6. Histograms of the astrometric HD 128311 residuals of the fit.

Table 12
Parallax and Proper Motions of HD 128311

| ID	Parallax	μ_x	μ_y
HST	60.532 ± 0.149	204.963 ± 0.162	−249.760 ± 0.143
HIP 2007[a]	60.60 ± 0.83	204.74 ± 0.74	−249.98 ± 0.61
HIP1997[b]	60.35 ± 0.99	205.46 ± 0.89	−249.68 ± 0.7
PPMXL[c]		205.1 ± 0.7	−249.7 ± 0.6

Notes.
[a] Perryman et al. (1997).
[b] van Leeuwen (2007).
[c] Roeser et al. (2010).

velocities. We use additional velocities to those in Wittenmyer et al. (2009), and have reduced all of the HET data set with our own independent reduction pipeline (shown in Table 4), so the values used in this paper are different and distinct from those presented in Wittenmyer et al. (2009).

We analyzed weighted Lomb–Scargle periodograms of the residuals from the following three fits: (1) only γ's fitted, (2) γ's and planet b fitted, and (3) γ's and planets b and c fitted. We looked for evidence of additional planetary periodic signals in these periodograms (see Figure 7). In the periodogram of the residuals to a Keplerian model that contains the planets b and c, we see a signal at ~11.22 days, and false alarm probability of 1.3×10^{-40}. A weighted Kepler periodogram (Zechmeister & Kürster 2009) had a signal at ~11.22 days with a false alarm probability of 3.7×10^{-65}. Even though the period at ~11.22 days had very high power, we performed a bootstrap randomization of the data set. We randomly shuffled the data, fixing the observation times for 100,000 trials. We assessed these shuffles with the same weighted Lomb–Scargle period-finding program, and in the interval between 11 and 11.5 days the highest power in any of the 100,000 randomized data periodograms was a single peak with probability of 3.35×10^{-04}, well below that of the actual data which was 3.7×10^{-65}. After modeling the signal found at 11.22 days as a planet,
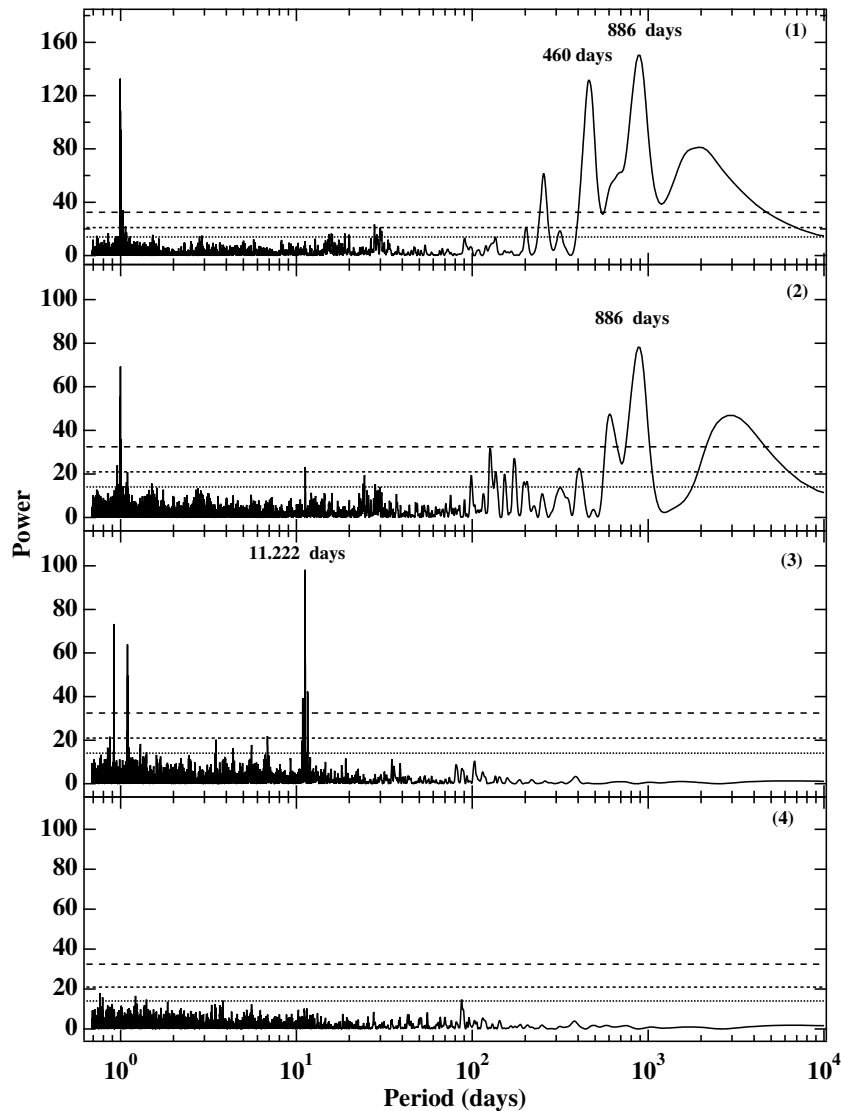
Figure 7. Periodogram of the radial velocity data of HD 128311 from two sources. Panel (1) shows peaks for planets b (460 days) and c (885 days). The false alarm probability of the peak at 460 days is 1.36×10^{-53} and the peak at 885 days is 1.22×10^{-61}. Panel (2) shows the periodogram of the residuals of a Keplerian model that contains planet b; planet c (period 885 days) can be seen. The false alarm probability of the peak at 885 days is 9.2×10^{-31}. Panel (3) shows the periodogram of the residuals of a Keplerian model that contains planets b and c; possible planet d (11.222 days) emerges. The false alarm probability of the peak at 11.222 days is 1.49×10^{-39}. Panel (4) shows the periodogram of the residuals to a Keplerian model that contains planet b (period 460 days), planet c (885 days), and planet d (11.222 days). The dotted lines show the significance levels of the power in each plot, from the top: 1.0×10^{-10}, 1.0×10^{-5}, and 1.0×10^{-2}.

Table 13
HD 128311 RV Modeling

| Model	χ^2	DOF	rms (m s^{-1})
No planets[a]	37125	443	77.11
b	9158	438	43.99
b + c	934	433	13.32
b + c + d	437	428	9.37

Note. [a] Solve for γ offsets only.

we find no other significant signals in the data set, as seen in panel (d). Finding no additional periodic signals to model from the periodograms in panel (d), we add a slope to the model to test for a longer period planet. We do not find a significant slope in this data set. Table 13 shows the χ^2, degrees of freedom (DOFs) and rms of the various HD 128311 independent RV planet modeling.

We look at a comparison of panel (a) from Figure 7 to a perfect data set created from the orbital fit of Table 14 with the precise epochs of our observational data shown in Figure 8 to investigate the orbital periods. The periodogram of the perfect data sets displays many of the features of the observational data sets, including the strong signal around a period of one day. The window function shown in Figure 9 shows that the peak at one day is due to sampling.

4.2.2. Simultaneous Radial Velocity and Astrometry Modeling

A combined GaussFit model was used to simultaneously model the astrometry and RV observations. (A review of Gauss-Fit being used for problems of linear regression with errors in both variables and the errors it produces is contained in Murtagh 1990.) Astrometric modeling of the target and reference frame consisted of scale, lateral color, cross-filter, proper motion, parallax, and the astrometric orbital elements of either planet c alone or planets b and c, and was carried out as detailed
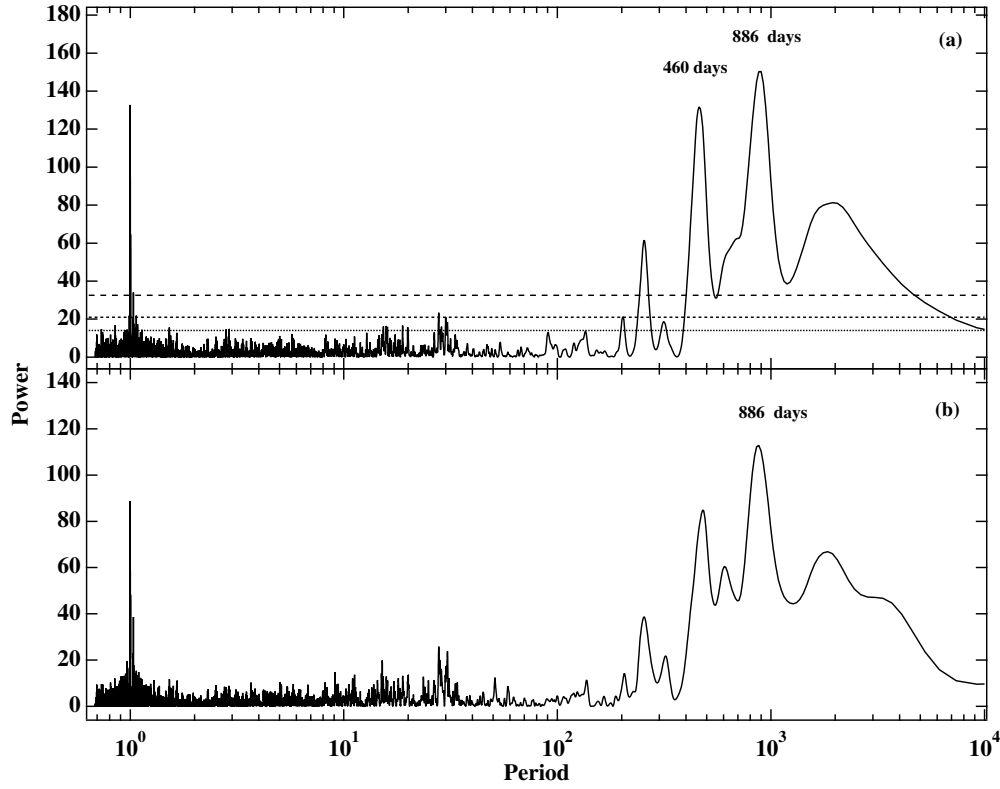
Figure 8. Periodogram of the radial velocity data of HD 128311 from two sources compared to a periodogram of perfect data. Both show periodograms of residuals with only γ fit. (a) Actual observational data shown in Figure 7(b) shows the periodogram of a simulated perfect data set for elements shown in Table 14. Panel (b) shows similar features to panel (a), including a peak around 1 day which must be due to sampling.

Table 14
HD 128311: Orbital Parameters and Masses

| Parameter	HD 128311 b	HD 128311 c	HD 128311 d
		RV	
K (m s^{-1})	55.627 ± 0.456	74.799 ± 1.497	13.982 ± 0.494
$HET\gamma$ (m s^{-1})	149.989 ± 0.661		
		Astrometry	
α (mas)		0.456 ± 0.092	
i (deg)	>30	55.950 ± 14.553	
Ω (deg)		229.392 ± 14.473	
		Astrometry and RV	
P (days)	453.019 ± 0.404	921.538 ± 1.15	11.2210 ± 0.0008
T[a] (days)	50198.691 ± 4.472	49565.615 ± 18.01	470736.315 ± 1.112
e	0.303 ± 0.011	0.159 ± 0.006	0.196 ± 0.030
ω (deg)	57.864 ± 3.258	15.445 ± 6.87	195.545 ± 8.66
		Derived[b]	
a (AU)	1.084 ± 0.006	1.740 ± 0.010	0.092 ± 0.004
Mass function ($M_\odot$)	6.99×10^{-09} $\pm 1.00 \times 10^{-10}$	3.84×10^{-08} $\pm 1.34 \times 10^{-09}$	2.99×10^{-12} $\pm 1.8 \times 10^{-13}$
$M \sin i$ (M_J)[c,d]	1.769 ± 0.023	3.125 ± 0.069	0.133 ± 0.005
M (M_J)[d]		$3.789 \,^{+0.924}_{-0.432}$	

Notes.

[a] $T = T - 2400000.0$.

[b] An HD 128311 mass of $0.828 \pm 0.012\ M_\odot$ (Takeda et al. 2007) was used in these calculations.

[c] The quantity referred to in radial velocity studies as mass, but is actually minimum mass.

[d] Masses are computed from an iteration of

$$\frac{m2^3}{(m1+m2)^2} = \frac{a^3}{P^2}. \qquad (12)$$
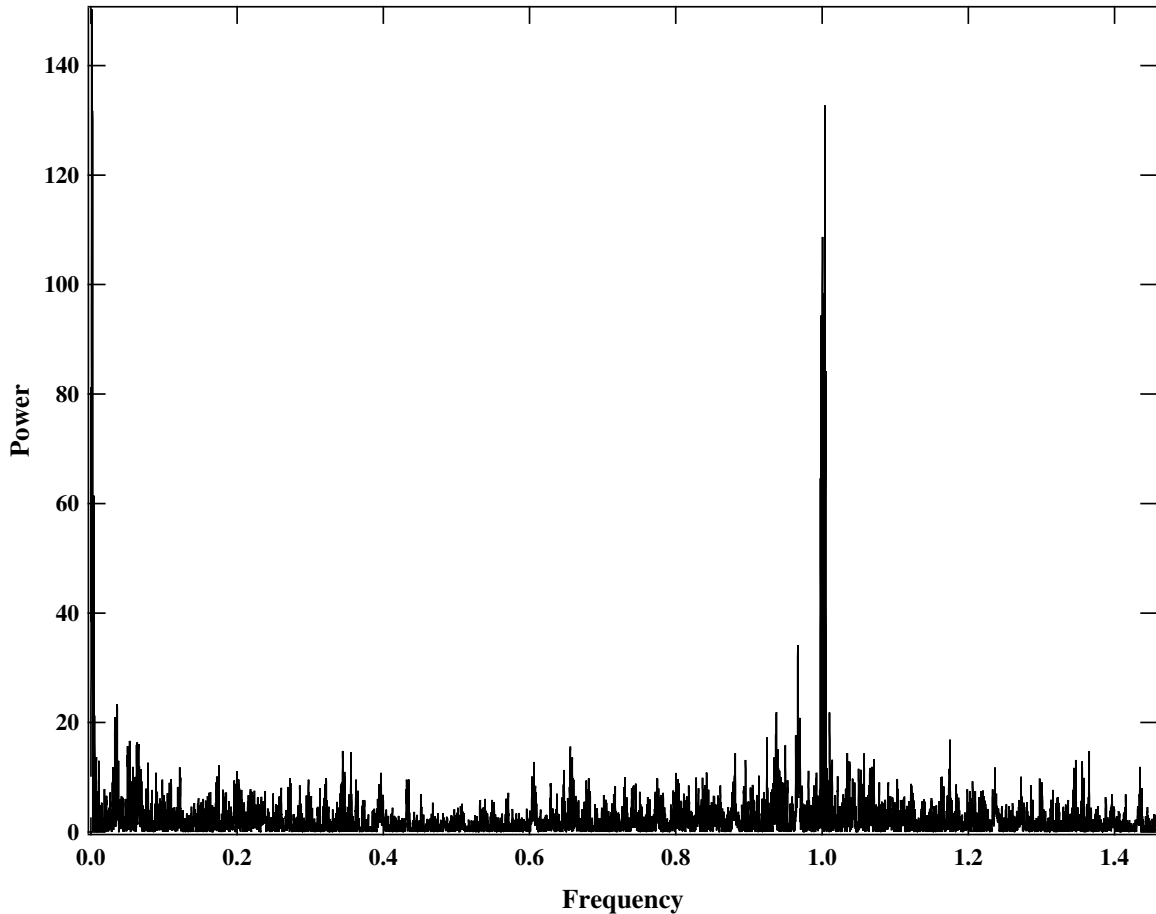
Figure 9. Window function of the radial velocity data of HD 128311 from two sources, showing a peak around one day due to sampling.

in Section 3.4. RV modeling of planets b–d was as detailed in Section 3.5. We constrained the relationship between the astrometry and RV with the equations shown in Section 3.6. We used a tolerance parameter in the GaussFit program that prevents a solution being found in shallow minimas. That tolerance parameter combined with the simultaneous modeling of free parameters (no parameters are held as constants) minimizes the chance of false detection.

Previous investigations (Benedict et al. 2002; McArthur et al. 2004, 2010; Bean et al. 2007; Martioli et al. 2010) and exploratory analysis have shown that we can conservatively detect astrometric signals larger than ∼0.25 mas. Of the two well-determined planets around HD 128311, only planet c would have an astrometric signal that would be detectable by the *HST* FGS at all inclinations (see Figure 10). Planet b could be detected if its inclination was less than 30°, and planet d could not be detected at any inclination by *HST* FGS.

One of the original motivations for these FGS observations was to assess coplanarity of HD 128311 b and c. Our attempt at the simultaneous modeling of planets b and c failed. With all parameters free, the program iterated endlessly rather than settling on a false detection, indicating that we were not able to detect planet b astrometrically. However, when we modeled only the astrometric signals of planets c with the same method, we detected the astrometric signal of planet c. As a test, we attempted to model the astrometric signal of planet b without c and that also failed. The simultaneous modeling of the orbital elements with the astrometry and the RV using GaussFit, with robust estimation, including the astrometric signal of planet c

lowered residuals over the same model which did not include the astrometric signal of planet c.

The orbital elements from this combined simultaneous solution are shown in Table 14 along with the derived elements. The uncorrelated one sigma errors shown are output from the Gauss-Fit program and are produced from a maximum-likelihood analysis of the classic "errors-in-variables" problem. Though not Bayesian, this technique (Jefferys 1990; Jefferys & Barnes 1999) can be regarded as an approximation to a Bayesian maximum a posteriori estimator with normal priors on certain parameters (see Section 3.4), without the inefficiency and questions of concluding convergence when Markov chain Monte Carlo methods are used.

Using classic astrometric elements to determine orbits does have some degeneracies. When the eccentricity equals zero, ω (argument of the node) and T (time of periastron) become indeterminate. When i (inclination) is equal to zero (face-on), the Ω (longitude of the node) becomes indeterminate. Looking at Table 14, we see that even with 3σ errors our determined eccentricities and inclination do not approach zero.

The condition number of a solution indicates the sensitivity of the result to errors (or changes) in the data or model. It gives you and upper bound on the degree to which the errors in the data are magnified in the result. The condition number for this combined model solution is $1.03 \times 10^{+1}$, which means the orbital solution is well constrained, and indicates a loss of only one significant digit in the result from the errors in the data and errors in the model.

13
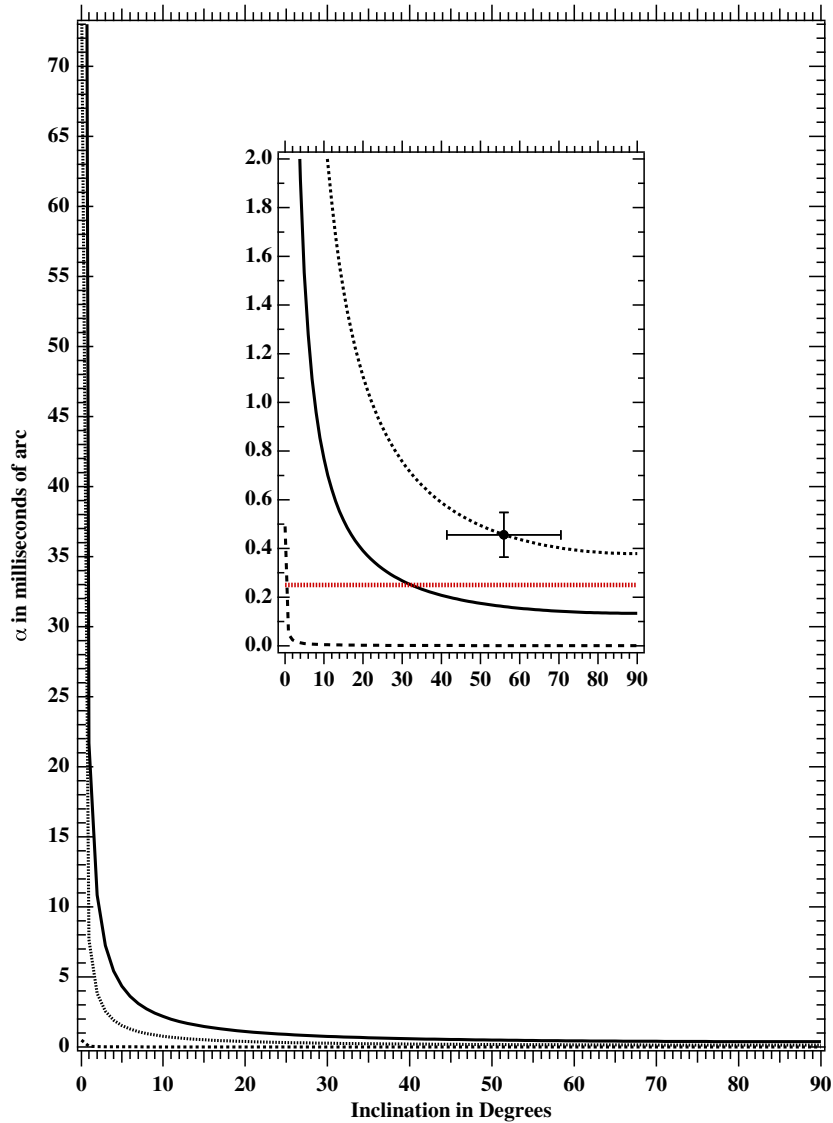
Figure 10. Astrometric α, perturbation, against inclination for the three planets in the HD 128311 system as calculated from Equation (8). The *HST* determined α for HD 128311 c is shown with error bars on the plots. The insert zooms in on components b and c and shows the detection limit of *HST* FGS (0.25 mas) in the horizontal dashed line.

(A color version of this figure is available in the online journal.)

The *HST* astrometric data error estimation is based upon a complex statistical examination of the raw data. We have chosen to continue to use these over-estimated errors because we are not able to assign the overestimation to a particular component of the complex error estimation process. Because of the overestimation of the astrometric data input errors, the actual errors of the astrometric parameters are most likely smaller than listed in the table.

We find the inclination of planet c to be $55°.95 \pm 14°.55$. This value is shown in Figure 10 with error bars, illustrating the constraint between astrometric and RV orbital parameters. We place a lower limit on the inclination of HD 128311 b of $30°$ based upon our inability to detect it in our modeling and our confidence in our detection limit. The astrometric motion of planet HD 128311 c against time is shown in Figure 11. The astrometric data shown in these plots (the dark filled circles) are normal points made from the HD 128311 residuals to an astrometric fit of the target and reference frame stars of scale, lateral color, cross-filter, parallax, and proper motion of multiple observations (light open circles) at each epoch.

To calculate companion masses, we use a stellar mass, $M_\star$, of $0.828^{+0.02}_{-0.01} M_\odot$ for HD 128311, which is a Bayesian-derived determination by Takeda et al. (2007), using the SPOCS catalog. We then find a minimum mass for planet b of 1.77 ± 0.02 $M_{\rm JUP}$ and actual an mass for planet c of $3.789^{+0.924}_{-0.432} M_{\rm JUP}$. The actual mass was derived from the *HST* astrometrically measured α's of planet c (0.456 ± 0.092). The minimum mass, $M \sin i$, for the possible planet d is 0.133 ± 0.005 $M_{\rm JUP}$. For possible planet d using Equation (1) of Bodenheimer et al. (2003), we find the probability of transit to be from 4%–5% dependent upon assumptions about planet d's radius and temperature.

The γ adjusted velocities from the HET and Lick observatories with the combined orbital fit of HD 128311 b, c and d over plotted are shown in the top panel of Figure 12 and the velocity residuals are shown in the lower panel. Table 15 shows the number of observations and rms of the two RV data sources with a weighted average rms of 9.37 m s^{-1}. The rms of the HET data was 8.37 m s^{-1}. Figure 13 shows the RV of companions b–d (with the other component velocities removed) plotted
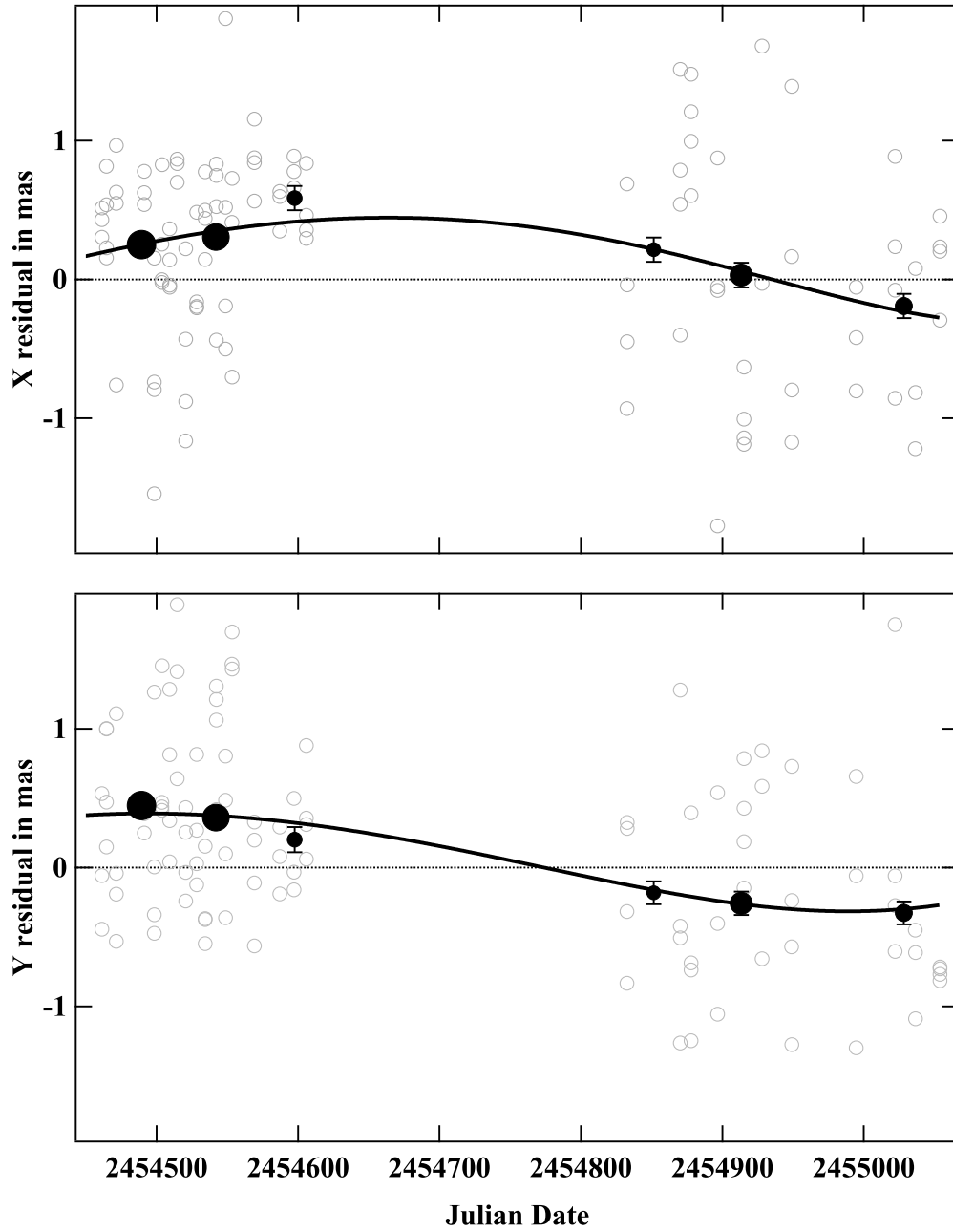
Figure 11. Astrometric reflex motion of HD 128311 due to c against time is shown. The astrometric orbit is shown by the dark line. Dark filled circles are normal points made from the HD 128311 residuals to an astrometric fit of the target and reference frame stars of scale, lateral color, cross-filter, parallax, and proper motion of multiple observations (light open circles) at each epoch. Normal point size is proportional to the number of individual measurements that formed the normal point. The peak-to-peak separation between the normal points, which are near peri- and apastron, is two times the perturbation semi-major axis (2α), by definition. Error bars represent the 1σ of the normal position. Many error bars are smaller than the symbols.

Table 15
Radial Velocity Data Sets of HD 128311

Data Set	Coverage	Number of Observations	rms (m s^{-1})
Lick	1998 June–2008 May	92	13.21
McDonald *HET*	2005 Apr–2011 Jan	355	8.37
Total		974	9.37

against orbital phase. The histogram in Figure 14 shows the Gaussian distribution of the HET RV residuals of the combined orbital model which include residuals from two different sources spanning 13 yr.

4.2.3. Proper Motion and Orbital Parameters in Astrometry

Black & Scargle (1982) suggested that the *linear* component of an astrometric perturbation (α) is absorbed into the proper motion and therefore both the period and amplitude of the orbital motion are underestimated unless several orbital cycles are observed. However, their hypothesis considers the astrometric orbit as being sinusoidal (circular, ecc = 0) and linear with time (see Figure 3 of Black & Scargle 1982). An eccentric orbit is not sinusoidal. A two-axis astrometric orbit with eccentricity is *never* linear in time. To test the Black and Scargle hypothesis, an "almost-perfect" data set was created with orbit, proper motion and observing times to match the
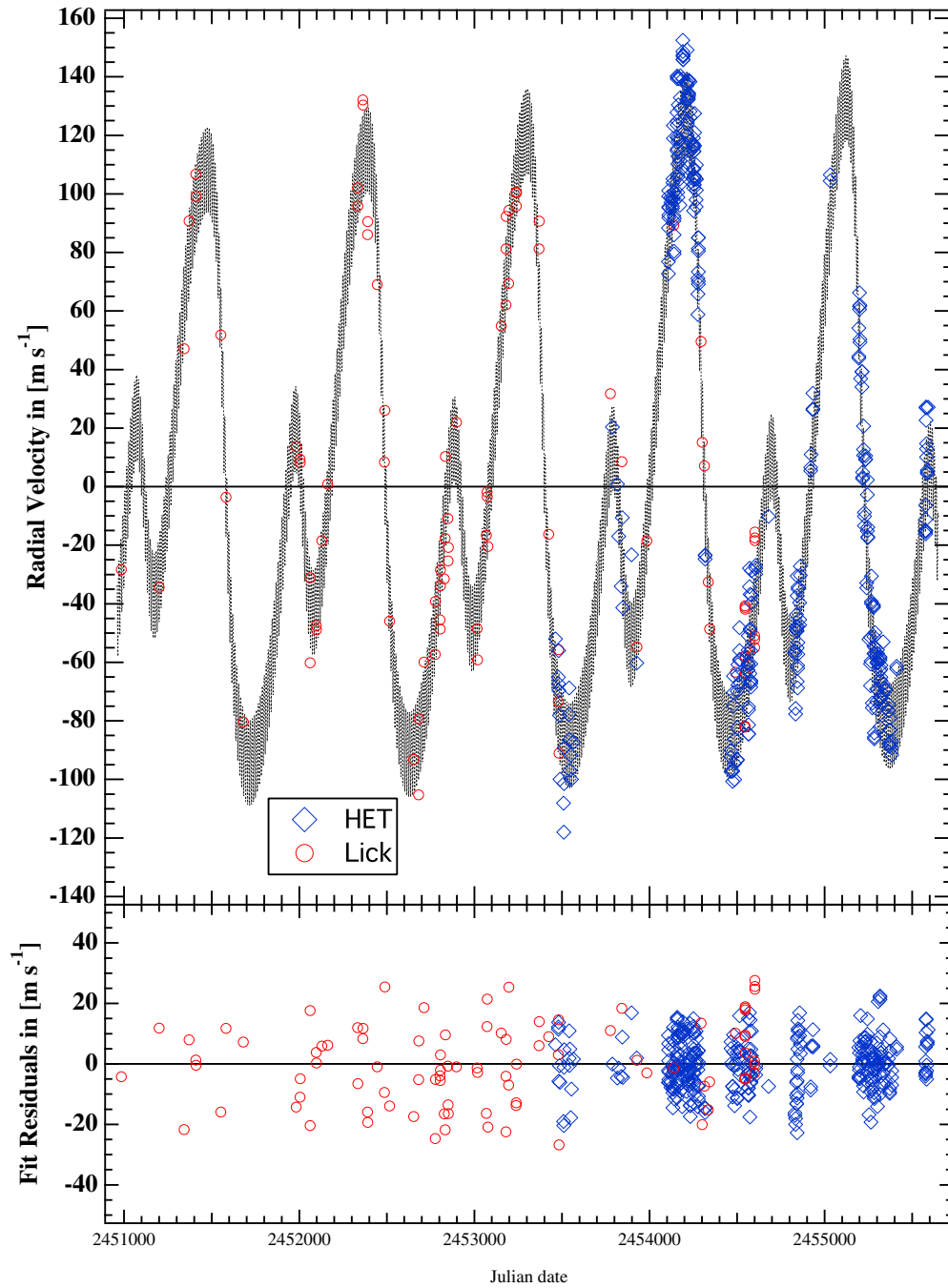
Figure 12. Radial velocities of HD 128311 vs. time from two sources. The orbital parameters were established with a simultaneous three-planet Keplerian orbit to all Doppler measurements combined with *HST* astrometry. The solid gray line shows the combined orbital fit which includes planets b, c, and d. The lower panel shows the residuals to the fit.

(A color version of this figure is available in the online journal.)

HST astrometry of HD 128311c. Without including the RV, and solving for all astrometric parameters simultaneously, we used our GaussFit model to determine the proper motion and orbital parameters, and compared the results with the input parameters to the fake data set of the proper motions and astrometric α. The μ_α difference was -3.377×10^{-6}, μ_δ difference was 1.532×10^{-6}, and the astrometric α difference was 1.309×10^{-6}, which are at the level of error in the fake data set. With 64% orbital coverage, we are able to recover the input parameters, without transfer of orbital motion into proper motion.

With accurate astrometric data, it is possible to determine orbital parameters with an arc of the orbit. It is only necessary to have enough astrometric data to be able to separate the nonlinearities of the orbital motion from the linear proper motion. Combining RV data of more than one period in a simultaneous model with the astrometry allows determination of astrometric parameters with observations times that stretch only one-tenth of the orbital period (Tuomi et al. 2009). The inclusion of the RV observations would also prevent absorption of the astrometric perturbation in a zero eccentricity orbit into the proper motions because the RV
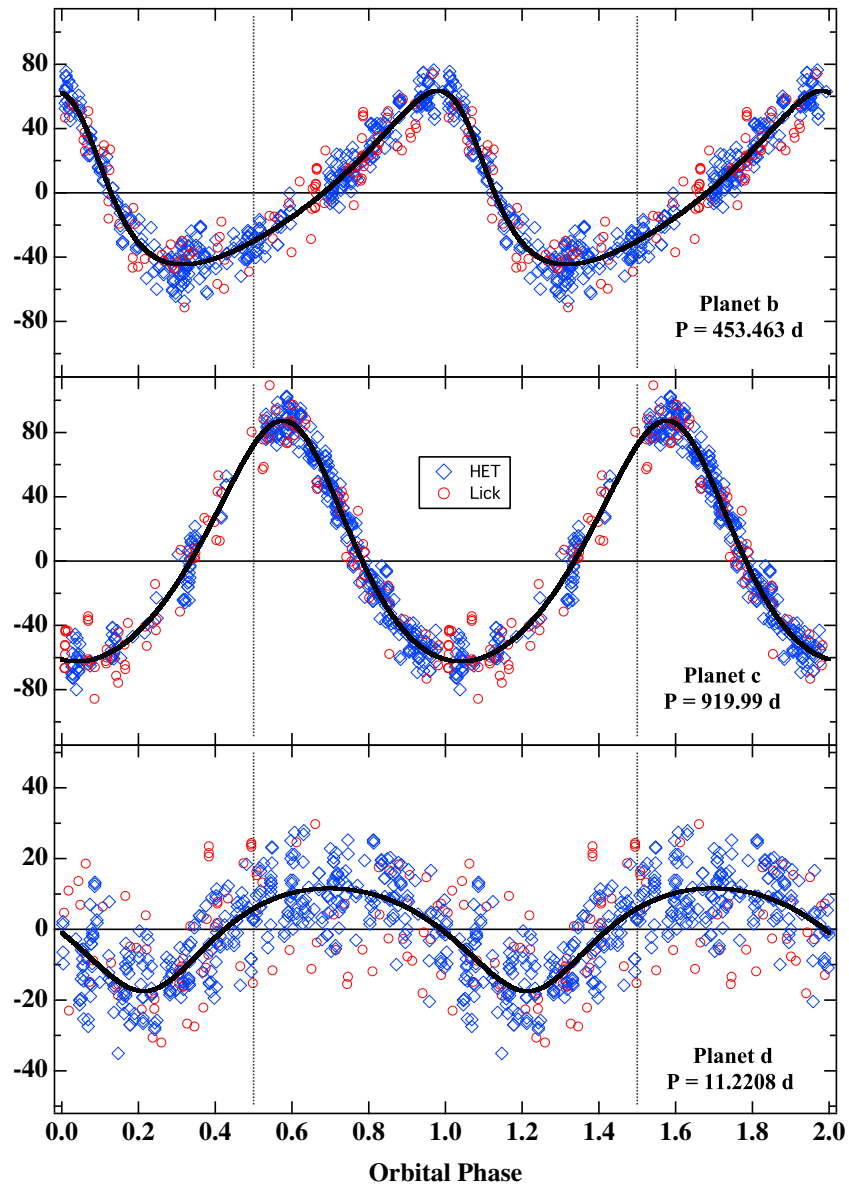
Figure 13. Residual velocities of HD 128311 vs. orbital phase for each planet after the subtraction of the signal produced by the two other planets. The orbital parameters were established with a simultaneous three-planet Keplerian fit to all Doppler measurements combined with *HST* astrometry. The solid line shows the Keplerian curve of the planet alone.

(A color version of this figure is available in the online journal.)

would constrain any period change that covaries with the α absorption.

4.2.4. Hipparcos versus HST Observations

Hipparcos astrometry measurements are inherently one-dimensional. *HST* astrometric measurements are two-axis interferometric. Several studies have shown that *Hipparcos* intermediate astronomic data (IAD) measurements do not have enough precision to determine planetary orbit, but can be used to set upper limits on planet size (Sozzetti 2005). However, with the re-reduction of the *Hipparcos* catalog in 2007 (van Leeuwen 2007), masses have been derived for substellar companions (Sozzetti & Desidera 2010; Reffert & Quirrenbach 2011). The technique used for these mass determinations uses the RV (spectroscopic) elements as constants and only solves for the astrometric *i* (inclination) and Ω (ascending node). The α (semi-major axis) is derived from a constraint with the spectroscopic elements held as constants (see Sozzetti & Desidera 2010, Equation (1)).

Because their semi-major axis is derived, Sozzetti & Desidera (2010) use Monte Carlo resamples to estimate the α error. The α is actually measured with the *HST* FGS observations in a simultaneous solution of all spectroscopic and astrometric elements, with the error directly calculated, as with the other parameters in the GaussFit model solution. Reffert & Quirrenbach (2011) did confirm the *HST* FGS results for ε Eri b (Benedict et al. 2006).

4.2.5. Modeling of the HST Astrometric Residuals

An noted in Section 4.2.2, the *HST* astrometric data is modeled for scale, lateral color, cross-filter, proper motion, and parallax. As an additional test of the astrometric signal, we model the astrometric data with the above parameters, but without the orbit of planet c and examine the residuals of that fit. We modeled the astrometric residuals (with reduced input errors) with a straight line fit in each axis over time, and with an orbit over time. The reduced χ^2 of the linear fit model was
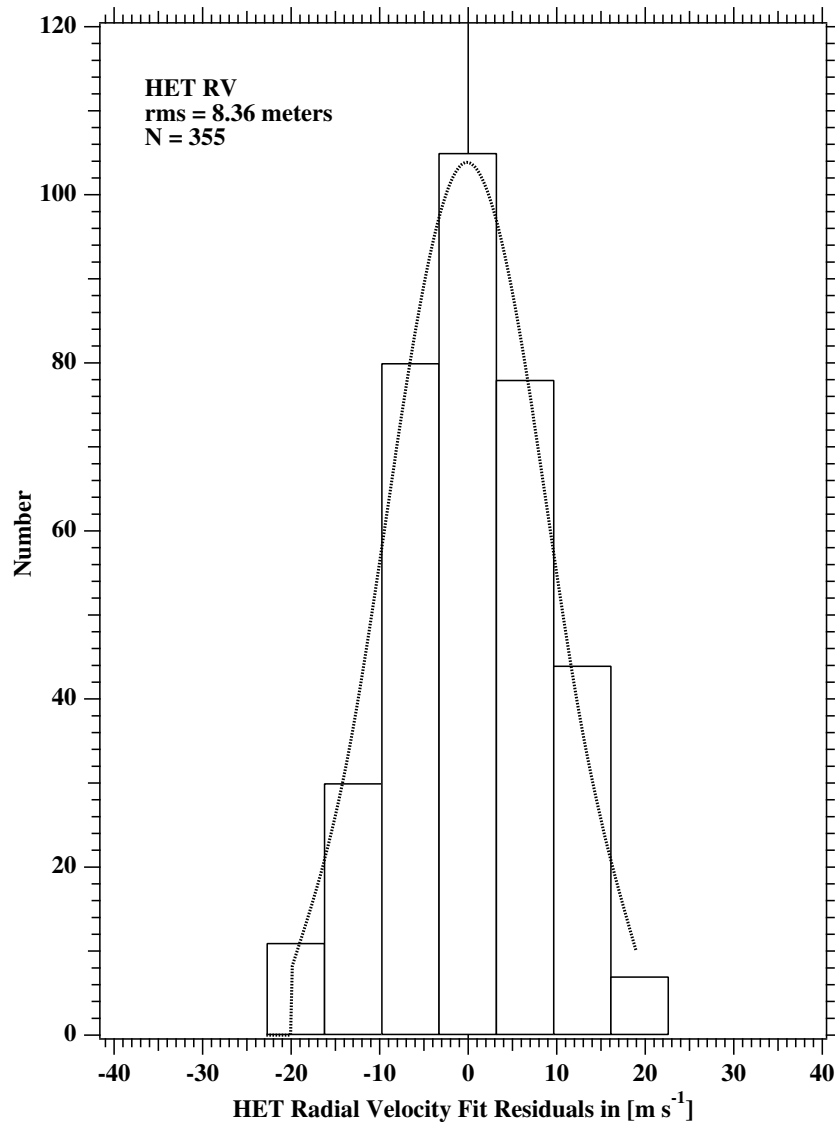
Figure 14. Histogram of the *HET* RV residuals of the simultaneous three-planet Keplerian Orbit fit to all Doppler measurements combined with *HST* astrometry of HD 128311.

14.17, while the reduced χ^2 of the orbital model was 3.00. The astrometric residual fit to an orbit was almost five times lower than the fit to a straight line, which supports the determination of an orbital signal in the residuals.
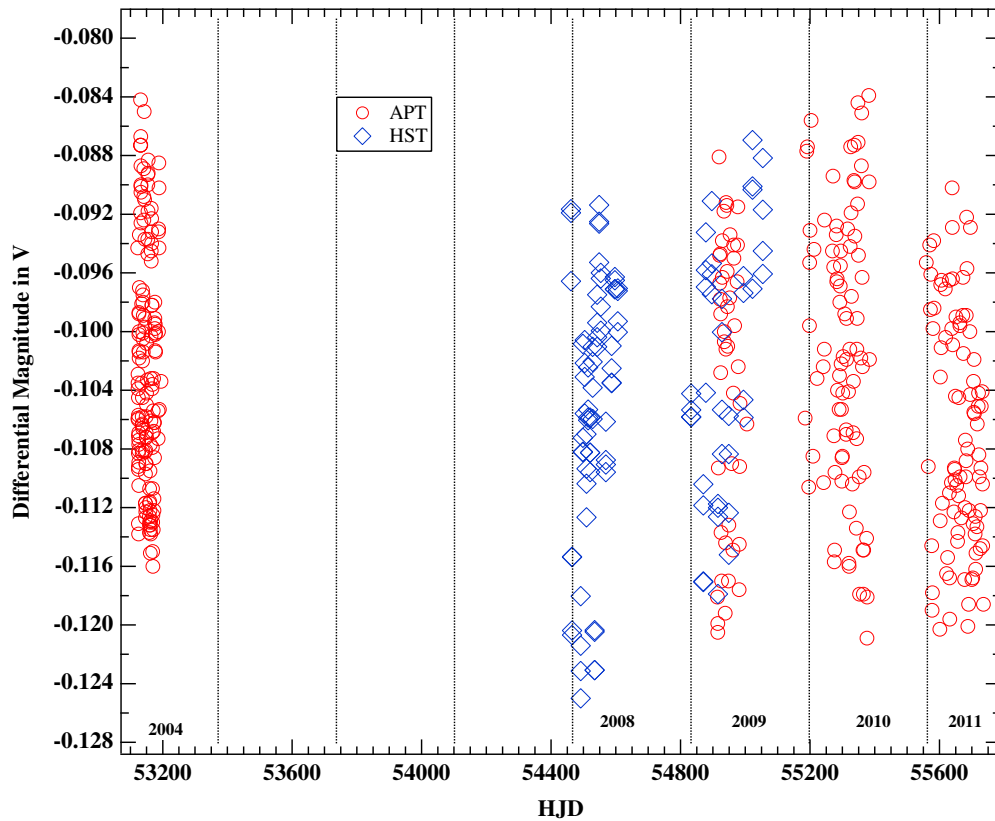
4.3. Photometry of HD 128311

In addition to our RV and astrometric observations described above, we acquired contemporaneous photometric observations of HD 128311 with the T12 0.80 m APT at Fairborn Observatory in southern Arizona. T12 is one of several Tennessee State University automatic telescopes in operation at Fairborn (Eaton et al. 2003). We also analyzed our astrometric observations with the *HST* FGS 1r, a millimag photometer (Benedict et al. 1998; Bean et al. 2008), to produce additional photometric observations simultaneous to the astrometric observations.

Precise photometric observations of planetary host stars are useful to look for short-term, low-amplitude brightness variability that may be the result of rotational modulation in the visibility of starspots and plages (see, e.g., Henry et al. 1995). Therefore, these observations can help to determine whether observed RV variations are caused by stellar activity or reflex

motion due to the presence of an orbiting companion. Queloz et al. (2001) and Paulson et al. (2004) have documented several examples of solar-type stars whose periodic RV variations were caused by stellar activity. Photometric observations of HD 128311 are of particular importance to establish the reality of the new 11.22 day planetary candidate HD 128311d seen in our RVs, given that Vogt et al. (2005) have suggested (from examination of Ca II H and K lines) that this active star has a rotation period of ∼12 days.

The T12 APT acquired 375 observations of HD 128311 during the 2004, 2008, 2009, and 2010 observing seasons. The T12 APT is equipped with a two-channel precision photometer employing two EMI 9124QB bi-alkali photomultiplier tubes to make simultaneous measurements in the Strömgren *b* and *y* passbands. The T12 APT and its two-channel photometer are nearly identical to the T8 APT described in Henry (1999). The APT was programmed to measure the brightness of HD 128311 (star *D*: $V = 7.48$, $B - V = 0.97$, K0) with respect to the three nearby comparison stars HD 129153 (star *A*: $V = 5.93$, $B - V = 0.24$, F0 V), HD 125752 (star *B*: $V = 7.97$, $B - V = 0.40$, F5), and HD 127247 (star *C*: $V = 7.41$,

Figure 15. Photometry from both the *HST* and T12 APT of HD 128311 against time in HJD. T12 APT are differential magnitudes and the *HST* FGS data have been offset to appear on the plot.

(A color version of this figure is available in the online journal.)

<div style="display:flex">

Table 16
HST Photometry of HD 128311

Julian Date	Magnitude
2454461.32336805	7.3987
2454461.33312499	7.3937
2454461.33790509	7.3984
2454464.51170138	7.3749
2454464.52334490	7.3699

(This table is available in its entirety in a machine-readable form in the online journal. A portion is shown here for guidance regarding its form and content.)

Table 17
*T*12 *APT* Photometry of HD 128311

Julian Date	Differential Magnitude
2453122.6862	−0.0943
2453123.7842	−0.106
2453123.8253	−0.1059
2453123.8326	−0.1029
2453123.8829	−0.1035

(This table is available in its entirety in a machine-readable form in the online journal. A portion is shown here for guidance regarding its form and content.)

</div>

$B - V = 0.53$, F2). Intercomparison of the various differential magnitudes of the four stars shows that comp star *A* is slightly variable over a range of a few millimagnitudes, comp stars *B* and *C* are constant to 0.001 mag or so, and our program star HD 128311 (star *D*) is variable over a range of ∼0.03 mag. Therefore, we created the most precise differential magnitudes of HD 128311 by averaging the $D - B$ and $D - C$ differential magnitudes into a single $D - (B + C)/2$ differential magnitude. We also combined our *b* and *y* observations into a single $(b+y)/2$ passband to improve the precision further. Finally, since the mean brightness of the four observing seasons varied slightly from year to year with a standard deviation of 0.0028 mag, we normalized each observing season to the same mean and computed the individual residuals from the mean. The four observing seasons of the APT data are plotted in Figure 17 with filled circles.

We combined the 108 *HST* FGS measurements listed in Table 16 spanning 1.62 yr with 375 additional observations from the T12 APT shown in Table 17 spanning (with gaps) 7.15 yr for the photometric analysis (see Figure 15). Typically the *HST* target star photometry is flat-fielded with the stars from its reference frame, but in the case of HD 128311 the only two reference stars that were in all of the observation sets were very faint reference stars with low pmt counts. The attempt to flat-field the data with these stars resulted in considerable noise being added to the data. Because we were unable to flat-field the data the *HST* photometry is expected to be of lower quality than usually produced. The *HST* magnitudes were derived from a relation between the sum of pmt counts of four channels with SIMBAD magnitudes of non-variable *HST* observed stars.

The Lomb–Scargle periodograms shown in Figure 16 of the *HST* photometry show a period of 11.1796 days with a probability of false detection of 1.223571×10^{-10} and T12
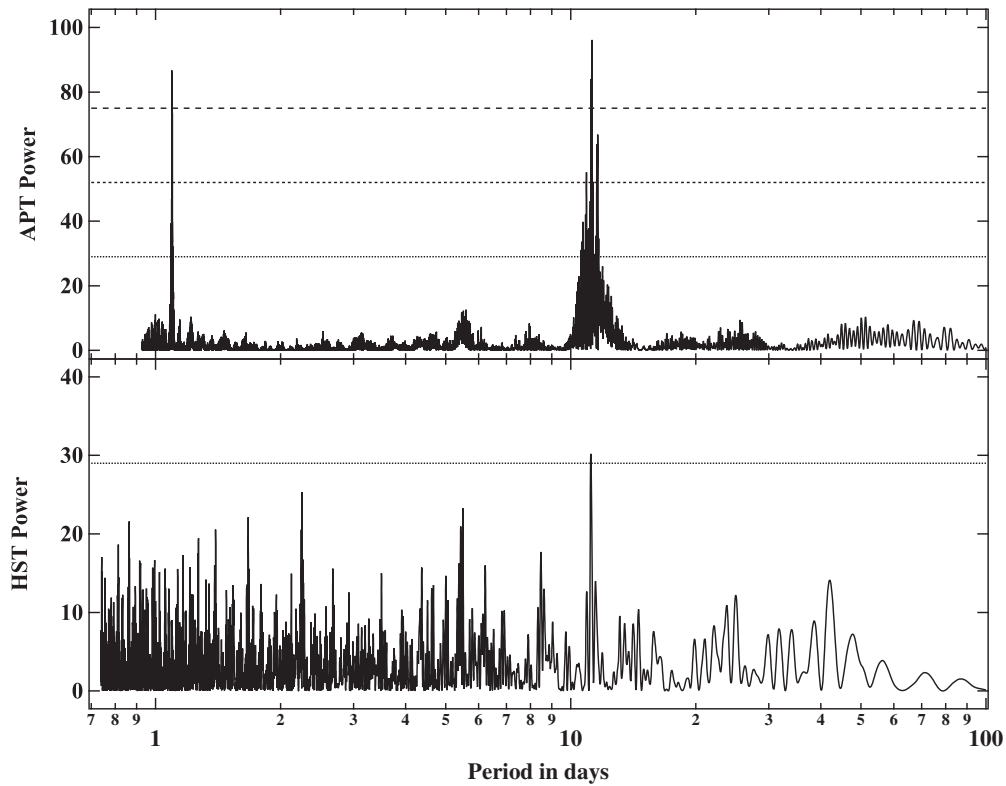
Figure 16. Periodogram of the photometry data of HD 128311 from two sources. Upper plot shows T12 APT photometry with a maximum peak at 11.248625 days and a false alarm probability of 9.854567×10^{-39}. The dotted lines show the significance levels of the power, from the top: 1.0×10^{-30}, 1.0×10^{-20}, 1.0×10^{-10}. Lower plots show *HST* photometry with a maximum peak at 11.179618 days and a false alarm probability of 1.223571×10^{-10}, only the significance level line of 1.0×10^{-10} is shown.

Table 18
Photometric Period Modeling of HD 128311

ID	Date	Period	Amplitude	rms	χ^2	DOF
T12 APT	Apr 4–Jul 4	11.33340 ± 0.03667	0.009 ± 0.001	0.00435	149	149
T12 APT	Mar 9–Jun 9	11.25298 ± 0.00099	0.012 ± 0.001	0.00478	53	41
T12 APT	Dec 9–Jul 10	11.25588 ± 0.00060	0.011 ± 0.001	0.0044	88	83
T12 APT	Dec 10–Jun 11	11.24745 ± 0.00055	0.009 ± 0.001	0.0041	79	86
HST	Dec 7–May 8	11.25000 ± 0.0000006	0.0117 ± 0.001	0.0069	44	64
HST	Jan 7–Aug 9	11.24999 ± 0.0000009	0.0101 ± 0.001	0.0069	19	37
Combined	Apr 4–Jun 11	11.25018 ± 0.0008	0.009 ± 0.0004	0.00054	583	468
Combined	Dec 7–Jun 11	11.25152 ± 0.0018	0.009 ± 0.0005	0.00054	466	317

APT photometric data showed a period of 11.2486 days with a probability of false detection of 9.854567×10^{-39}. GaussFit was used for simple phase modeling of the photometric data from both instruments using this equation:

$$\Phi = a + b * \Delta t + A * \sin\left(\frac{2 * \pi * \Delta t}{P}\right), \qquad (9)$$

where a is an offset and b is a linear trend term for each season of data (four for T12 APT and one for *HST*), Δt is the change in time, A is the amplitude of the sine wave, and P is the period in days of the photometry.

While there is an indication from comparing a polynomial fit to the sine fit of the photometric data that there are subtle low level differences, the sine wave photometric model appears to be adequate for the period determination. Adding an eccentric component to the sine fit did not improve the results. Table 18 lists the period of each season separately and simultaneously, along with the rms of the fit and DOF and χ^2. The 2004 T12

APT data is much noisier in regard to the period determination as can be seen from the table. We did allow for a single time offset in the Julian Dates of the observations from the two instruments.

Figure 17 shows the coherent photometric signal in sequential time. It is interesting that the modeled period derived from *HST* photometry is significantly different than the result from the periodogram and closer to that derived from the T12 APT data. The photometric period found in the modeling of all epochs of both data sets is $P_{\text{phot}} = 11.25145 \pm 0.00046$ days. For the simultaneous modeling of both sets of data the variance (σ^2) used for the T12 APT data was 2.6×10^{-5}, while the variance used for the *HST* data was 1.95×10^5. In the top panel of Figure 18 we see both sources of photometric data phased to this period. The lower panel shows all photometric data phased to the period of the d component RV variations ($P_{\text{RV}} = 11.2210$ days). While the periods of the photometry and the RV are very similar, they are not the same within the errors.
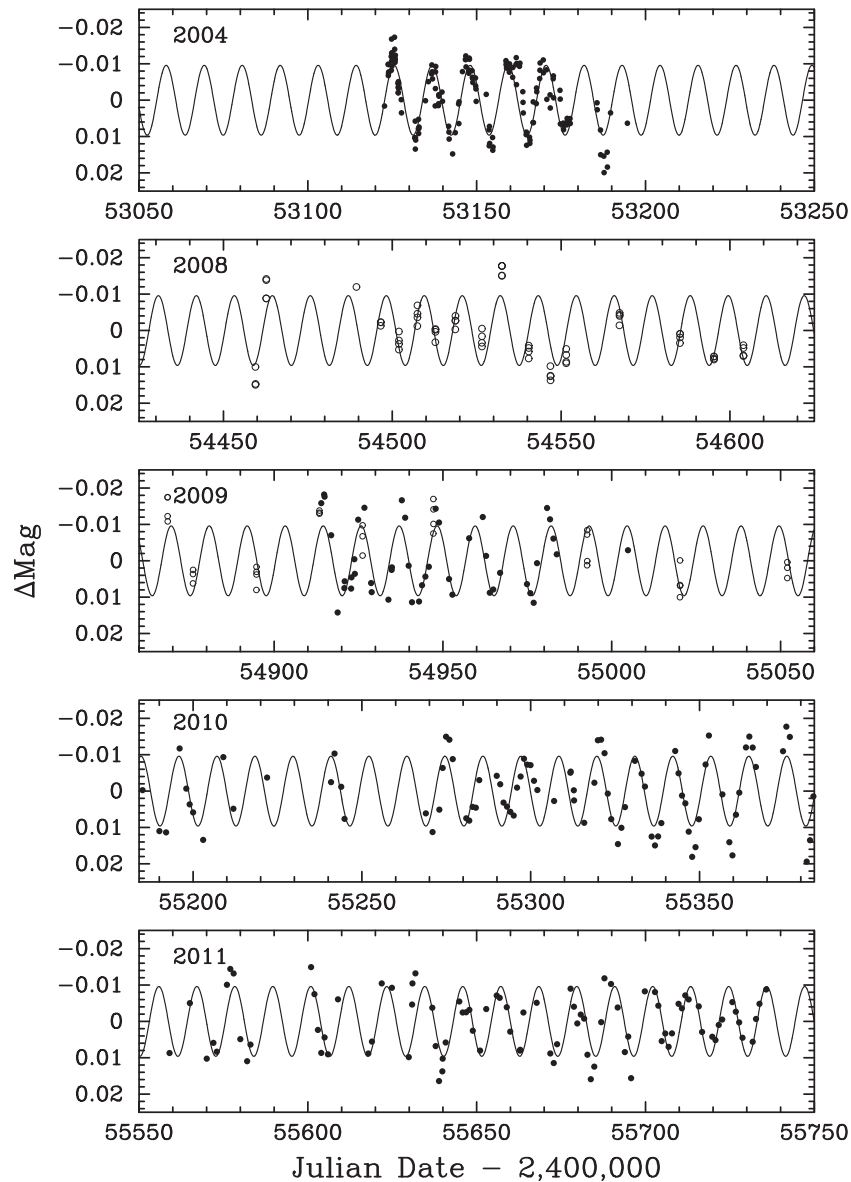
Figure 17. Plot of the photometry data of HD 128311 from two sources against time by year showing coherency over 8 yr. The peak-to-peak amplitude of the fitted sine curve is 0.01920 ± 0.00066 mag. The filled circles in the plot are APT data. The open circles are the *HST* data.

### 4.4. Cross-correlation Bisector Analysis

In order to assess the origin of short period RV variations we performed a bisector analysis on data from the HET. We found that on one of the two observing tracks of the HET close to twilight there were very large outliers in bisector span measurements as shown in Figure 19. The magnitude of the bisector span outliers was much larger than the uncertainty attributed to these observations in the RV reduction process. We removed these western track, near twilight observations from our RV and bisector data sets.

Because of the similar photometric and RV periods (P_{phot}, P_{RV}), we examined the bisector of the cross-correlation function (CCF) of 274 HET RV observations to look for correlations with the 11.2210 day RV period. We look for distortions in the CCF bisector that occur because of the movement of starspots across the limbs of the star as it rotates. We used the method of Johns–Krull (see Mahmud et al. 2011; Huerta et al. 2008, for recent discussions). The bisector spans and offsets were determined by cross correlating 12 orders covering the

wavelength range 4387–4847 Å. The values represent the mean CCF bisector span computed from the CCF of the 12 orders and the error is the standard deviation in the mean of the 12 orders. We found no correlation between the CCF bisector spans and the RV residuals (Figure 20). We did find a correlation between the bisector span uncertainties and the day of the year and track of the observations at the HET and used these to filter the higher noise HET data as explained in Section 3.1.

4.5. Dynamical Stability Analysis

Early dynamic work (Vogt et al. 2005) suggested that the system parameters derived from the Lick RV measurements most certainly required resonance for stability. Our new analysis uses Mercury (Chambers 1999) with a wrapper STAB (by Martioli) that provides a method for automatically inputting orbital elements with uncertainties that are incremented by either a Gaussian or uniform distribution. Unfortunately, Mercury does not implement the effects of general relativity, which could affect the stability of the system. Therefore, we can expect that
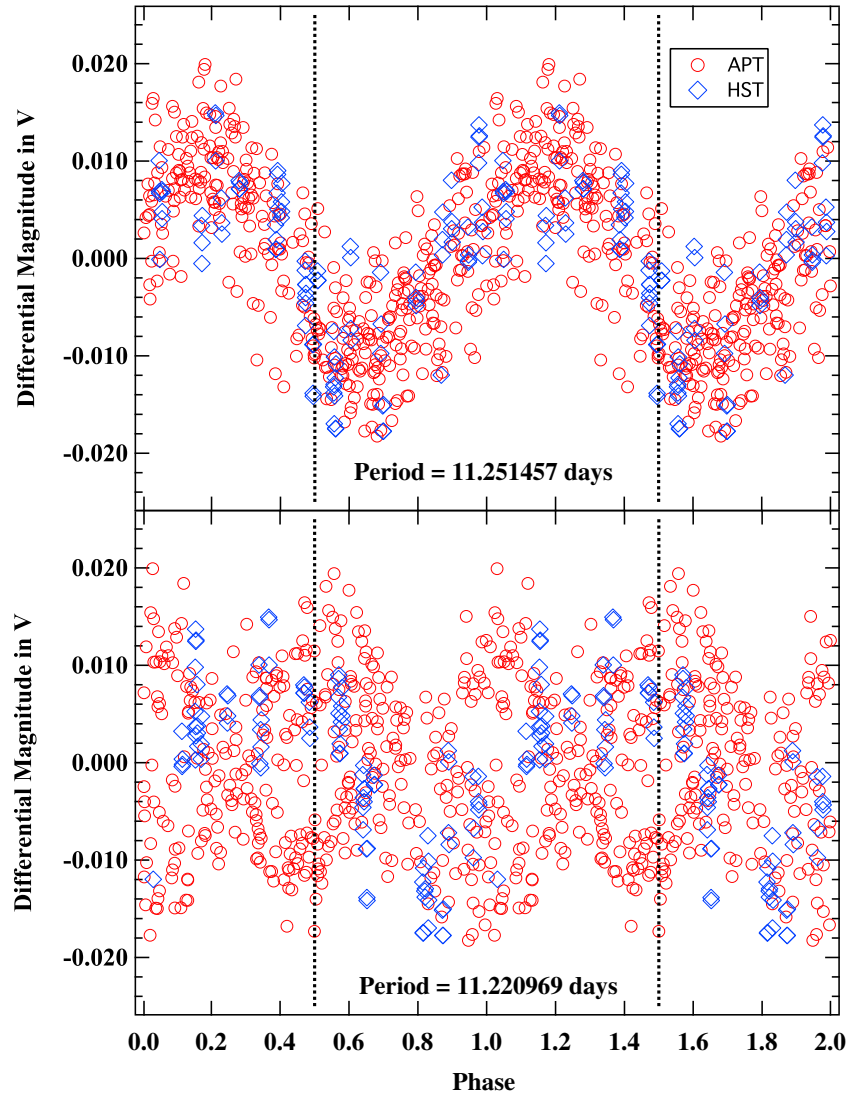
Figure 18. Phase plot of the photometry data of HD 128311 from two sources. Upper plot shows T12 APT and *HST* photometry phased to the photometry modeled period of 11.25145 days. The lower plots show T12 APT and *HST* photometry phase to the radial velocity signal of 11.220969 days.

(A color version of this figure is available in the online journal.)

these initial results may present a more minimal picture of the regions of stability in the dynamical map.

In this preliminary investigation, we used the astrometric and RV elements and errors in Table 14 for HD 128311 for planets b and c as inputs into STAB (STAB converts the orbital elements into canonical coordinates). We use the Bullrisch–Storer integration, with time steps of 22 days, and a Julian day start time of 2453462.0 and stop time of 3654953462.00 days. We found stability for the system for 10 million years.

To examine the claim of resonance in the HD 128311 system we looked at the ψ's calculated with this equation:

$$\psi = p * M_1 - q * M_2 - (p - q) * \varpi_{1or2}, \qquad (10)$$

where $p = 2$, and $q = 1$ for this system, M is the mean longitude, and ϖ is the longitude of pericenter. We see in Figure 21 that the resonant angles are circulating, which indicates that there is no resonance. If the system were in resonance, all the data would be confined to a certain range on the y-axis (usually, but not always 0° or 180°).

5. DISCUSSION

5.1. Possible Coplanar Architecture

The astrometric data set for the determination of orbital parameters of HD 128311 was less robust than our past data sets for complex multi-planet systems. We had only 29 orbits in contrast to the 54 orbits we had for υ Andromedae, and these orbits were interrupted by several months for observing constraints, producing a data gap. The measurements were spread out over time with none of the intense monitoring that we had for υ Andromedae. We were only able to observe at maximum parallax factors twice due to *HST* instrumental restrictions on telescope roll, we had a large 225 day gap in the middle of our observation set, and our reference frame was very faint, with data losses on different stars in different orbits. All of these things combined produced a less than optimum data set. Nevertheless, we did find an inclination of planet c of $55°95 \pm 14°55$ and were able to place a lower limit on the inclination of HD 128311 c of 30°. These measurements support the possibility of coplanar architecture for HD 128311 b and c.
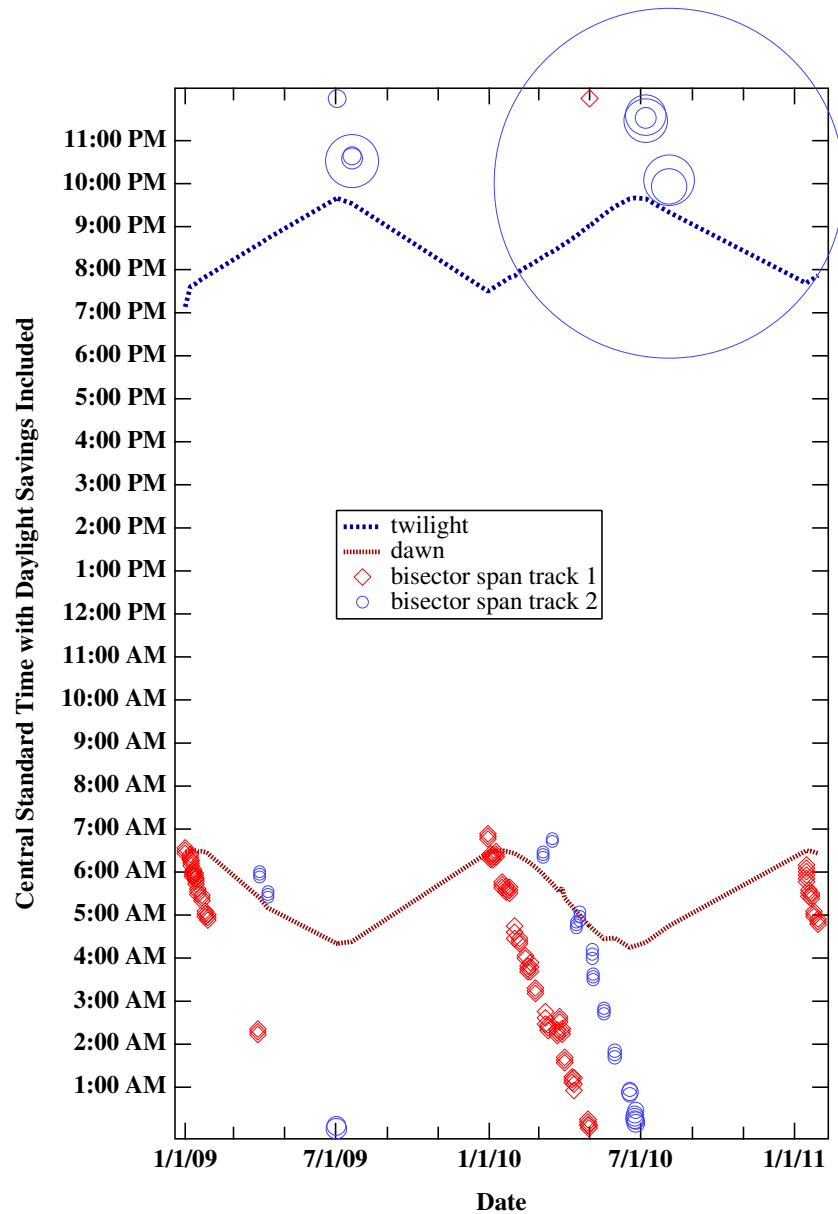
Figure 19. Results of bisector span analysis of HET radial velocity data of HD 128311 plotted against date and time. Time is shown as central standard time with daylight saving included. Twilight and dawn are indicated. The HET has two tracks—track 1 (◇) when azimuth is approximately 110° (E) and track 2 (○) with an azimuth of approximately 240°(W). Symbol sizes indicate bisector span size. Large outliers exist near twilight on track 2 (W). These outliers (large circles at the top of the figure) were removed from the HET radial velocity data set.

(A color version of this figure is available in the online journal.)

### 5.2. Detection of an Additional Planet or Activity Cycle?

In active stars, rotational modulation of surface phenomenon or pulsations can mimic RV variations that are due to reflex motions induced by planetary companions. The signature of rotational modulations are usually sinusoidal and varying over time (because of the growth and decay of the individual starspots) and are identified by periodogram analysis of the measured S (Ca II H and K index) values (although there can be phase shifts between the S value variation and the RV variation). We were not able to compute a Mount Wilson "S" index because our HET HRS spectrum do not cover the wavelength region of the Ca II H and K lines.

RV and photometric variations with periods of a few days due to pulsations have been detected in K-type stars, but these are all giant stars (Hatzes & Cochran 1993, 1994). Stellar pulsations with periods of a few days in a K dwarf, which HD 128311 is, would be unprecedented and there is only one (USNW-V-760) unconfirmed report of possible pulsations in such a star (Koen 2011, 2012). From a theoretical study of the radial pulsations of low mass stars (Gabriel & Grossman 1977), the pulsation period of the K dwarf would be expected to be much shorter than the observed photometric variation ($P_{phot} = 11.25145$) we see in HD 128311.

Because of concerns about planet detection around active stars, Butler et al. (2003) evaluated Mount Wilson Ca II H and K S-values of HD 128311 from their Keck spectra and only found two periods at 31 and 25 days that were close to the 1% false alarm probability. They also suggested that monitoring of the system would show excursions from the Keplerian
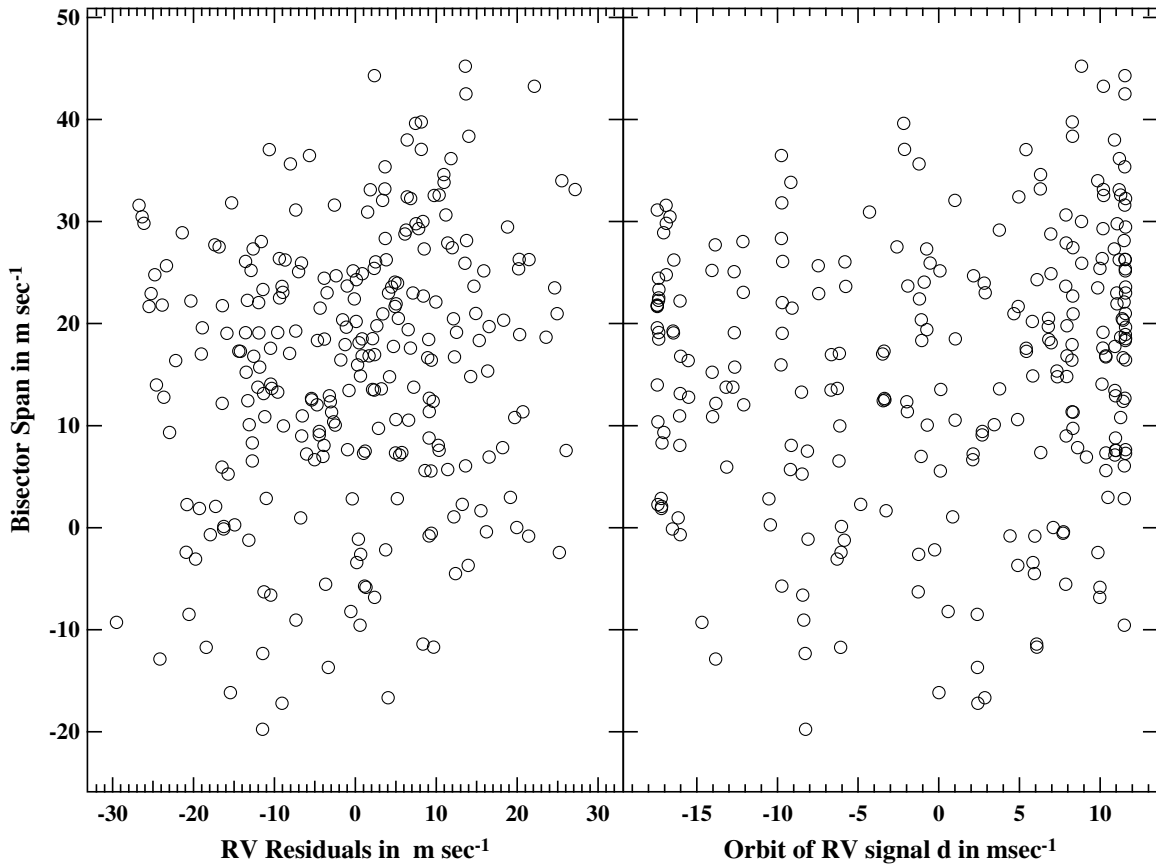
Figure 20. Plot of the bisector spans and radial velocity fit residuals of HD 128311 and a perfect orbit. A correlation between the bisector spans and the radial velocity residual would indicate star activity as the source of the radial velocity variations. Left panel shows the bisector spans against the radial velocity residual after the fit of components b and c. Right panel shows the bisector span against the modeled radial velocity signal of possible companion d, to minimize the noise of the actual observations. Lack of correlation suggests a planetary origin.

orbit, if the RV variation were being caused by other star phenomenon.

In the followup announcement of the discovery of the second planetary body in the system, Vogt et al. (2005) found strong evidence of a RV periodicity at 5.6 days and speculated that this period was caused by spots on opposite hemispheres of the stars rotating across the disk. Strassmeier et al. (2000) had first identified a photometric period 11.5 days with an amplitude of 0.035 mag. Vogt et al. (2005) later found a period of 11.53 ± 0.15 days with 0.03 mag amplitude in photometric variability. They predicted the rotation period to be $P_{rot} = 12$ days from emission at Ca II H and K, which they found it to be in agreement with the photometric period of 11.53 days, which also explained to them the 5.6 day RV period.

As discussed in Section 4.2.1, after removal of the two known planets b and c, a strong RV signal remains at 11.22 days which can be seen in Figure 7. This period is twice that of the 5.6 day period found by Vogt et al. (2005) in the residuals to their two planet fit. We do not see the shorter 5.6 signal in our periodogram (see Figure 7) or in a plot of residuals to a two planet fit phased to 5.6 days. The HET data set has much higher cadence over a significant period of time compared to the Lick data (see Figure 12). We found a significant drop of over 50% in the χ^2 of the solution with the addition of the Keplerian orbit planetary argument c to the model, shown in Table 13.

Because the origin of the RV variations was not related with certainty to the photometric variability we turned to additional

methods of discernment. Bisectors of spectral lines (Gray 1976; Hatzes et al. 1997) or the CCF's can be examined to rule out rotational modulations of starspots and non-radial pulsations. If there is asymmetry in the CCFs that is correlated with the RV variations, then a planetary companion can be ruled out. Without correlation, radial pulsations or a planetary companion can still be considered. In the case of HD 128311 radial pulsations are unlikely at the period of the RV signals. In the past, after further examination, tentative planets in HD 166435 (3.7987 days; Queloz et al. 2001) and more recently BD +20 1790 (Hernán-Obispo et al. 2010; Figueira et al. 2010) were ruled out when the RV variations proved to be due to stellar activity. Chromatic variations that result in RV amplitude that is wavelength dependent can also be indicators that the signal is caused by rotational modulation or pulsations.

We proceeded with additional examinations of the photometry (see Section 4.3) and bisectors (see Section 4.4) to determine the origin of the residual periodic RV observations. T12 APT and *HST* photometry showed a robust photometric period of $P_{phot} = 11.25145 \pm 0.00046$ days which is very close, but not within the errors to RV period of $P_{RV} = 11.2210 \pm 0.0008$. We see the that the photometry is much more compelling phased to the period determined by it rather than by the RV P_{RV} (see Figure 18).

If HD 128311 is a low amplitude starspot variable, the coherency of the time period of the photometric observations is unusual. Starspots in these types of stars typically appear
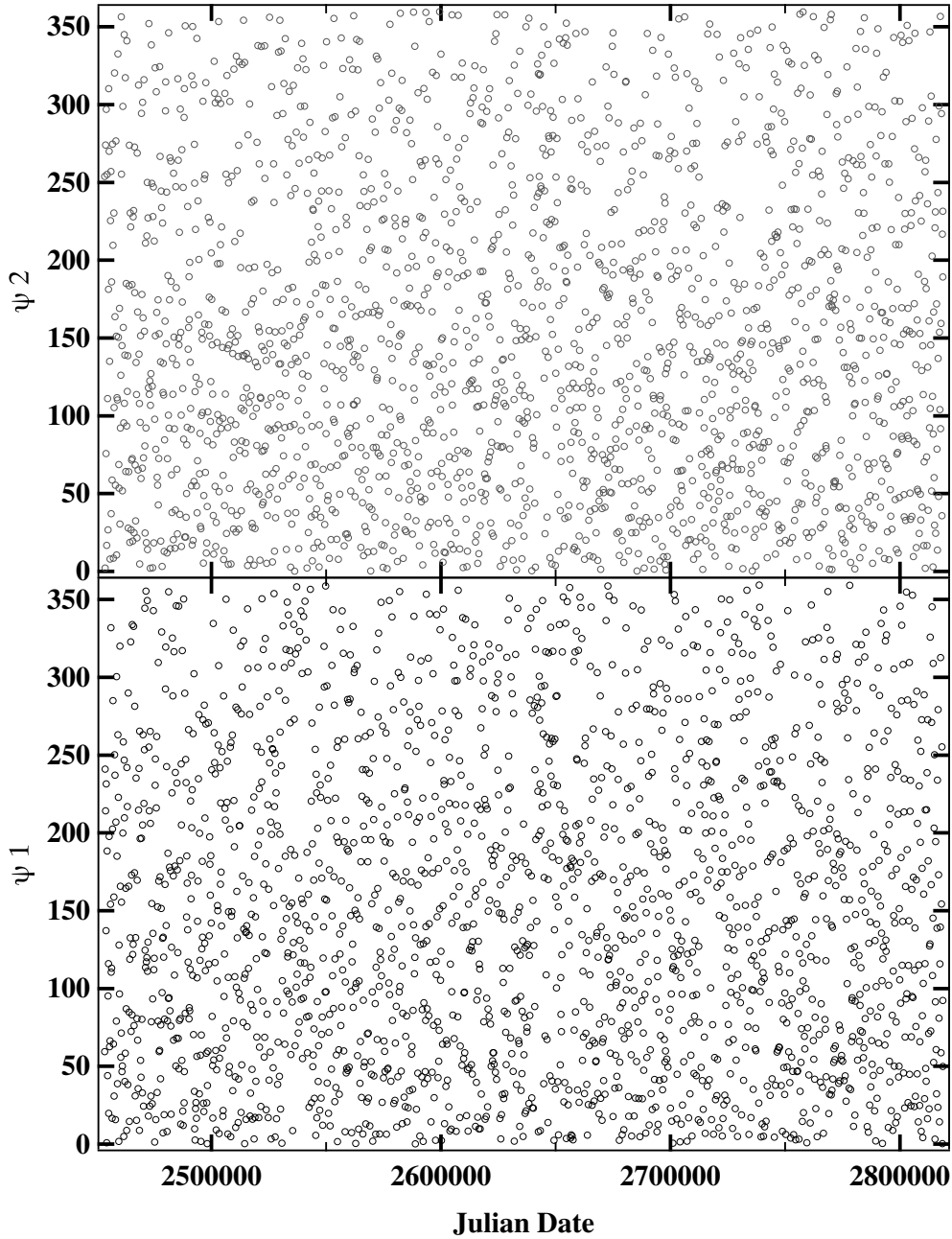
Figure 21. Plot of ψ derived with Equation (10) from the dynamical integration of elements from the solution shown in Table 14 of the HD 128311 system. ψ is circulating, so we do not see the libration that indicates that HD 128311 b and c are in mean motion resonance.

more as scatter plots, when phased over time (Henry et al. 1995, 2002). Using this equation,

$$P_{\text{ROT}} = \frac{2 * \pi * R_\star}{v \sin i}, \qquad (11)$$

and $R_\star = $ of 0.76 $R_\odot$ (from Table 1), and the $v \sin i = 3.65$ km s^{-1} (from Table 2) we find at an inclination of 90° a rotation period of 10.53 ± 1.46 days, and even shorter if the inclination is less than 90°. If the rotation period is considerably shorter, then we must find an explanation for a rotation period that is shorter than the stable photometric period.

We then turned to our examination of bisectors (Section 4.4). Instead of using individual spectra to calculate bisectors, we computed a CCF which is expected to be more robust. We

examined 274 observations to minimize the chance of an anomalous observation dominating the result. Figure 20 shows no correlation between the CCF bisector span and the RV measurements. While it has been shown that there are cases where lack of correlation between bisectors and the RV is not evidence for a planet, Desort et al. (2007) in simulations and Prato et al. (2008) in practice showed that these cases involved stars where the $v \sin i$ is close to or lower than the visible light spectral resolution of the RV observations. In the case of HD 128311, the $v \sin i$ of 3.65 km s^{-1} is close, but larger than ($2*v \sin i$) the spectral resolution of the HET/HRS ($R = 60,000$) of around 5 km s^{-1}.

While it is tempting to attribute the RV period to the stellar photometric activity or starspots, questions remain as to whether that is a viable explanation. This type of star does not exhibit

radial pulsations at either 12 days or the shorter ~6 day period, so we can remove radial pulsations from consideration. The RV orbit determined for HD 128311 d is eccentric. The photometric variation of HD 128311 is much more stable over a relatively long term of photometric observations that is expected in this type of star. The periods of the RV and photometry are very close but not the same within the errors with large volumes of data analyzed.

One possible explanation for the two observed periods is the presence of differential rotation. We know that HD 128311 is an active, solar-like star so it is reasonable to expect that different latitudes of the star rotate at different periods. Furthermore, if the observed RV and photometric variations are dominated by spots at different stellar latitudes one should see slightly different periods. For instance, if we assume a solar differential rotation law then the spots that dominate the RV and photometric variations would only have to differ in latitude by about 6°.

The lack of correlation between RV and bisector span measurements argues against the spot scenario, but it is not clear if the bisector span measurements are of sufficient quality to be conclusive on this issue. The expressions of Saar & Donahue (1997) and Hatzes (1996) result in an estimated amplitude for the bisector span variations of ≈ 7 m s^{-1}, yet the rms scatter of the bisector span variations is about 20 m s^{-1}, or about a factor of three larger. Given the long-lived coherent nature of the photometric variations and its slight difference in period between it and the RV variability, the nature of the 11.2 day RV period is still open. Continued photometric and spectroscopic monitoring of this star is needed to resolve this issue.

It is difficult to explain the long-term stability of the photometry being due to starspots in this type of star in which the rotation period may be shorter. Finally, we do not see correlation between the CCF of the bisectors and the RV, correlation would support starspots or non-radial pulsations. The activity is not likely induced by tidal forces because we would expect the photometric period to be one-half the rotation period. Magnetic interaction producing photometric variations between the possible HD 128311 d component and the star has not been found in other K star hot Jupiter systems with even shorter periods. If we have indeed found HD 128311 d and we have an established photometric period that is unusual in nature for this star type, then a mechanism for the relationship between this object and the activity would be interesting and provocative.

5.3. Are HD 128311 b and c in Resonance?

The system parameters for HD 128311 derived from the early Lick RV measurements proved to be unstable in dynamical integrations (Vogt et al. 2005). A 2:1 MMR for HD 128311 b and c was invoked for stability purposes. Using additional data, Meschiari et al. (2009) derived a Newtonian best fit with the systemic program, but found those orbital parameters were also unstable over a short time period. Further investigations with a bootstrap Monte Carlo procedure of trial fits finally reported a stable fit that was protected by a 2:1 MMR, with a θ_1 librating with an amplitude of ~60° and a circulating $\delta\omega$. However (Voyatzis et al. 2009) using the Butler et al. (2006) orbit, found evidence of libration in all three angles θ_1, θ_2, and $\delta\omega$ of 43°, 83°, and 103°. Theory suggested that planet–planet scattering was a pathway to the supposed resonance (Barnes & Greenberg 2006a, 2006b; Raymond et al. 2008). While others produced (Rein & Papaloizou 2009) a simulation based upon the 2005 Vogt et al. (2005) elements that had stochastic forcing from turbulence and migration but no presence of "rogue" planets.

This suggested that stochastic forces due to turbulence can alter, but not disrupt MMRs. More recently, Lecoanet et al. (2009) reiterated the conclusion of an earlier paper by Adams et al. (2008) that MMRs should be rare, and classified the status of 2:1 MMR of HD 128311 as unresolved.

In contrast to the earlier Keplerian and Newtonian solutions to the available Lick data, with the addition of the large set of HET observations and *HST* data, and the modeling of an additional signal HD 128311 d, we find a Keplerian solution (see Table 14) that is stable for 10 million years and upon examination, does not show evidence of MMR (see Figure 21), offering support to the conclusions of Adams et al. (2008) and Lecoanet et al. (2009) that MMR's should be rare.

5.4. Modeling of the Additional Radial Velocity Signal

Evidence seems to suggest that the third signal, HD 128311 d, found in the RV data set may be a viable planetary candidate. Even if it were some sort of lagging response to the photometric signal, we have modeled it in the RV data, removing its noise from the orbital parameters of HD 128311 b and c, and produced an orbital architecture that presents contrasting results with previous investigations. Instead of instability, we now have stability for 10 million years, and instead of a theory of MMR in this system, we find no evidence of that in our examination of the ψ's. Modeling all signals found in our data leads to a very different look at the architecture of this exoplanetary system.

5.5. The Importance of Astrometric Followup of Extrasolar Systems

The astrometric determination of the mass of a low-mass companion can decisively characterize it as a planet and reveal its hierarchical position in a planetary system. A good illustration of this fact can be seen from the results of our group for two objects that were previously listed as extra-solar planet candidates: Gliese 876 b and HD 136118 b. Surprisingly each object has been found to belong to a different class: a giant planet and a brown dwarf (Benedict et al. 2002; Martioli et al. 2010). These results demonstrate the importance of the application of complementary techniques in observing extra-solar planetary systems.

6. CONCLUSIONS

We have combined 355 new high-cadence RV measurements from the HET, 92 adjusted existing observations from Lick, 112 *HST* FGS astrometric and photometric observations, and 375 T12 APT photometric observations to clarify the architecture and dynamics of the extrasolar planetary system around the K dwarf star HD 128311. We have updated a result found in the previous Lick data set for υ Andromedae. We offer these final observations.

1. We find an inclination of $55°.95 \pm 14°.55$ and a true mass of $3.789 ^{+0.924}_{-0.432}$ M_{JUP} for HD 128311 c and a lower limit on the inclination of HD 128311 b of 30°, which could support a coplanar architecture for the system. We have assumed Gaussian errors in the data, and the orbital solution, which is nonlinear, is a local approximation regarding the Gaussian nature of the errors in the parameters we determine.

2. We find an additional RV signal in the data, with a period of $P_{\mathrm{RV}} = 11.2210 \pm 0.0008$ days and eccentricity of 0.204 ± 0.030, which could be an additional planet d, with a minimum mass of 0.136 ± 0.007 M_{JUP}. Bisector analysis does not confirm stellar activity as the origin of the signal.

3. We find a consistent long-term photometric signal that is atypical of this type of star that has a period of $P_{\mathrm{phot}} = 11.25145 \pm 0.00046$ days, that is very close to, but not within the errors of the RV signal.

4. We find dynamic stability for a span of 10 million years adopting the orbital parameters derived in this paper using Mercury with Bullrisch–Storer integration.

5. We find no evidence of MMR from examination of the ψ's in this system with the orbital parameters presented in this paper.

6. We find a parallax of 60.532 ± 0.149 mas for HD 128311 in good agreement with, but with much lower errors of those found with *Hipparcos* data.

7. We find that the additional planet found by Curiel et al. (2011) in the previously published data for υ Andromedae is a result of γ offsets that have since been discovered in the Lick data.

REFERENCES

Adams, F. C., Laughlin, G., & Bloch, A. M. 2008, ApJ, 683, 1117
Bailer-Jones, C. A. L. 2011, MNRAS, 411, 435
Barnes, R., & Greenberg, R. 2006a, ApJL, 652, L53
Barnes, R., & Greenberg, R. 2006b, ApJ, 638, 478
Barnes, S. A. 2007, ApJ, 669, 1167
Bean, J. L., Benedict, G. F., Charbonneau, D., et al. 2008, A&A, 486, 1039
Bean, J. L., McArthur, B. E., Benedict, G. F., et al. 2007, AJ, 134, 749
Beaugé, C., Michtchenko, T. A., & Ferraz-Mello, S. 2006, MNRAS, 365, 1160
Beichman, C. A., Bryden, G., Rieke, G. H., et al. 2005, ApJ, 622, 1160
Beichman, C. A., Bryden, G., Stapelfeldt, K. R., et al. 2006, ApJ, 652, 1674
Benedict, G. F., McArthur, B., Nelan, E., et al. 1998, AJ, 116, 429
Benedict, G. F., McArthur, B. E., Feast, M. W., et al. 2007, AJ, 133, 1810
Benedict, G. F., McArthur, B. E., Forveille, T., et al. 2002, ApJL, 581, L115
Benedict, G. F., McArthur, B. E., Gatewood, G., et al. 2006, AJ, 132, 2206
Bessell, M. S., & Brett, J. M. 1988, PASP, 100, 1134
Black, D. C., & Scargle, J. D. 1982, ApJ, 263, 854
Bodenheimer, P., Laughlin, G., & Lin, D. N. C. 2003, ApJ, 592, 555
Bryden, G., Beichman, C. A., Carpenter, J. M., et al. 2009, ApJ, 705, 1226
Butler, R. P., Marcy, G. W., Vogt, S. S., et al. 2003, ApJ, 582, 455
Butler, R. P., Marcy, G. W., Williams, E., et al. 1996, PASP, 108, 500
Butler, R. P., Wright, J. T., Marcy, G. W., et al. 2006, ApJ, 646, 505
Carpenter, J. M. 2001, AJ, 121, 2851
Castelli, F., Gratton, R. G., & Kurucz, R. L. 1997, A&A, 318, 841
Chambers, J. E. 1999, MNRAS, 304, 793
Cox, A. N. 2000, Allen's Astrophysical Quantities (4th ed.; New York: AIP)
Crida, A., Sándor, Z., & Kley, W. 2008, A&A, 483, 325
Curiel, S., Cantó, J., Georgiev, L., et al. 2011, A&A, 525, A78

Desort, M., Lagrange, A. M., Galland, F., et al. 2007, A&A, 473, 983
Donahue, R. A. 1993, PhD thesis, New Mexico State Univ.
Droege, T. F., Richmond, M. W., Sallman, M. P., et al. 2006, PASP, 118, 1666
Eaton, J. A., Henry, G. W., & Fekel, F. C. 2003, The Future of Small Telescopes in the New Millennium, Vol. 2 (Dordrecht: Kluwer)
Érdi, B., Nagy, I., Sándor, Z., et al. 2007, MNRAS, 381, 33
Figueira, P., Marmier, M., Bonfils, X., et al. 2010, A&A, 513, L8
Fischer, D. A., Marcy, G. W., Butler, R. P., et al. 2003, ApJ, 586, 1394
Fischer, D. A., & Valenti, J. 2005, ApJ, 622, 1102
Gabriel, M., & Grossman, A. S. 1977, A&A, 54, 283
Gayon, J., & Bois, E. 2008, A&A, 482, 665
Gayon-Markt, J., & Bois, E. 2009, MNRAS, 399, L137
George, S. J., & Stevens, I. R. 2007, MNRAS, 382, 455
Giuppone, C. A., Beaugé, C., Michtchenko, T. A., et al. 2010, MNRAS, 407, 390
Gonzalez, G., & Laws, C. 2007, MNRAS, 378, 1141
Gould, A., & Morgan, C. W. 2003, ApJ, 585, 1056
Goździewski, K., & Konacki, M. 2006, ApJ, 647, 573
Gray, D. F. 1976, The Observation and Analysis of Stellar Photospheres (Research supported by the National Research Council of Canada; New York: Wiley), 484
Gray, R. O., Corbally, C. J., Garrison, R. F., et al. 2003, AJ, 126, 2048
Hatzes, A. P. 1996, PASP, 108, 839
Hatzes, A. P., & Cochran, W. D. 1993, ApJ, 413, 339
Hatzes, A. P., & Cochran, W. D. 1994, ApJ, 432, 763
Hatzes, A. P., Cochran, W. D., & Johns-Krull, C. M. 1997, ApJ, 478, 374
Heintz, W. D. 1978, Double Stars (Dordrecht: Reidel)
Henry, G. W. 1999, PASP, 111, 845
Henry, G. W., Donahue, R. A., & Baliunas, S. L. 2002, ApJL, 577, L111
Henry, G. W., Fekel, F. C., & Hall, D. S. 1995, AJ, 110, 2926
Hernán-Obispo, M., Gálvez-Ortiz, M. C., Anglada-Escudé, G., et al. 2010, A&A, 512, A45
Huerta, M., Johns-Krull, C. M., Prato, L., et al. 2008, ApJ, 678, 472
Jefferys, W. H. 1990, Biometrika, 77, 597
Jefferys, W. H., & Barnes, T. G. 1999, in Bayesian Statistics 6, ed. J. Bernardo, J. Berger, A. Dawid, & A. Smith (Oxford: Oxford Univ. Press), 777
Jefferys, W. H., Fitzpatrick, M. J., & McArthur, B. E. 1988, CeMec, 41, 39
Kashyap, V. L., Drake, J. J., & Saar, S. H. 2008, ApJ, 687, 1339
Koen, C. 2011, MNRAS, 411, 813
Koen, C. 2012, MNRAS, 419, 706
Lawler, S. M., Beichman, C. A., Bryden, G., et al. 2009, ApJ, 705, 89
Lecoanet, D., Adams, F. C., & Bloch, A. M. 2009, ApJ, 692, 659
Lee, M. H., & Thommes, E. W. 2009, ApJ, 702, 1662
Mahmud, N. I., Crockett, C. J., Johns-Krull, C. M., et al. 2011, ApJ, 736, 123
Maldonado, J., Martínez-Arnáiz, R. M., Eiroa, C., et al. 2010, A&A, 521, A12
Mannings, V., & Barlow, M. J. 1998, ApJ, 497, 330
Martioli, E., McArthur, B. E., Benedict, G. F., et al. 2010, ApJ, 708, 625
McArthur, B., Benedict, G. F., Jefferys, W. H., et al. 1997, in The 1997 *HST* Calibration Workshop with a New Generation of Instruments, ed. S. Casertano, R. Jedrzejewski, T. Keyes, & M. Stevens (Baltimore, MD: Space Telescope Science Institute), 472
McArthur, B., Benedict, G. F., Jefferys, W. H., et al. 2002, in The 2002 HST Calibration Workshop : Hubble after the Installation of the ACS and the NICMOS Cooling System, ed. S. Arribas, A. Koekemoer, & B. Whitmore (Baltimore, MD: Space Telescope Science Institute), 373
McArthur, B. E., Benedict, G. F., Barnes, R., et al. 2010, ApJ, 715, 1203
McArthur, B. E., Benedict, G. F., Jefferys, W. J., et al. 2006, in The 2005 HST Calibration Workshop: Hubble After the Transition to Two-Gyro Mode, ed. A. M. Koekemoer, P. Goudfrooij, & L. L. Dressel (Greenbelt, MD: Goddard Space Flight Center, NASA), 396
McArthur, B. E., Endl, M., Cochran, W. D., et al. 2004, ApJL, 614, L81
Meschiari, S., Wolf, A. S., Rivera, E., et al. 2009, PASP, 121, 1016
Michtchenko, T. A., Beaugé, C., & Ferraz-Mello, S. 2008, MNRAS, 387, 747
Moro-Martín, A., Malhotra, R., Bryden, G., et al. 2010, ApJ, 717, 1123
Murtagh, F. 1990, in Errors, Bias and Uncertainties in Astronomy, ed. C. Jaschek & F. Murtagh (Cambridge: Cambridge Univ. Press), 385
Nelan, E. P. 2007, Fine Guidance Sensor instrument Handbook (16th ed.; Baltimore, MD: STScI)
Paulson, D. B., Saar, S. H., Cochran, W. D., et al. 2004, AJ, 127, 1644
Perryman, M. A. C., Lindegren, L., Kovalevsky, J., et al. 1997, A&A, 323, L49
Piskunov, N. E., & Valenti, J. A. 2002, A&A, 385, 1095
Pourbaix, D., & Jorissen, A. 2000, A&AS, 145, 161
Prato, L., Huerta, M., Johns-Krull, C. M., et al. 2008, ApJL, 687, L103
Queloz, D., Henry, G. W., Sivan, J. P., et al. 2001, A&A, 379, 279
Quillen, A. C. 2006, MNRAS, 365, 1367
Ramírez, I., & Meléndez, J. 2005, ApJ, 626, 465
Raymond, S. N., Barnes, R., Armitage, P. J., et al. 2008, ApJL, 687, L107

Reffert, S., & Quirrenbach, A. 2011, A&A, 527, A140
Rein, H., & Papaloizou, J. C. B. 2009, A&A, 497, 595
Ribas, I., Solano, E., Masana, E., et al. 2003, A&A, 411, L501
Rocha-Pinto, H. J., & Maciel, W. J. 1998, MNRAS, 298, 332
Roeser, S., Demleitner, M., & Schilbach, E. 2010, AJ, 139, 2440
Saar, S. H., & Donahue, R. A. 1997, ApJ, 485, 319
Saffe, C., & Gómez, M. 2004, A&A, 423, 221
Saffe, C., Gómez, M., & Chavero, C. 2005, A&A, 443, 609
Saffe, C., Gómez, M., Pintado, O., et al. 2008, A&A, 490, 297
Sándor, Z., & Kley, W. 2006, A&A, 451, L31
Sándor, Z., Kley, W., & Klagyivik, P. 2007, A&A, 472, 981
Schlegel, D. J., Finkbeiner, D. P., & Davis, M. 1998, ApJ, 500, 525
Sozzetti, A. 2005, PASP, 117, 1021
Sozzetti, A., & Desidera, S. 2010, A&A, 509, A103
Standish, E. M., Jr. 1990, A&A, 233, 252
Strassmeier, K., Washuettl, A., Granzer, T., et al. 2000, A&AS, 142, 275
Takeda, G., Ford, E. B., Sills, A., et al. 2007, ApJS, 168, 297
Tanner, A., Beichman, C., Bryden, G., et al. 2009, ApJ, 704, 109
Trilling, D. E., Bryden, G., Beichman, C. A., et al. 2008, ApJ, 674, 1086

Tull, R. G. 1998, Proc. SPIE, 3355, 387
Tuomi, M., Kotiranta, S., & Kaasalainen, M. 2009, A&A, 494, 769
Tuomi, M., Pinfield, D., & Jones, H. R. A. 2011, A&A, 532, A116
Valenti, J. A., & Fischer, D. A. 2005, ApJS, 159, 141
van Altena, W. F., Lee, J. T., & Hoffleit, E. D. 1995, The General Catalogue
    of Trigonometric [Stellar] Parallaxes (4th ed.; New Haven, CT: Yale Univ.
    Observatory) (YPC95)
van Belle Gerard, T., & von Braun, K. 2009, ApJ, 694, 1085
van Leeuwen, F. 2007, Hipparcos, the New Reduction of the Raw Data
    (Astrophysics and Space Science Library, Vol. 350; Berlin: Springer)
Vogt, S. S., Butler, R. P., Marcy, G. W., et al. 2005, ApJ, 632, 638
Voyatzis, G., Kotoulas, T., & Hadjidemetriou, J. D. 2009, MNRAS,
    395, 2147
Wittenmyer, R. A., Endl, M., Cochran, W. D., et al. 2009, ApJS, 182, 97
Wright, J. T., Upadhyay, S., Marcy, G. W., et al. 2009, ApJ, 693, 1084
Yong, D., & Lambert, D. L. 2003, PASP, 115, 796
Zacharias, N., Finch, C., Girard, T., et al. 2009, yCat, 1315, 0
Zacharias, N., Monet, D. G., Levine, S. E., et al. 2004, BAAS, 36, 1418
Zechmeister, M., & Kürster, M. 2009, A&A, 496, 577